MOX–Report No. 06/2013

Isogeometric Analysis for second order Partial Differential Equations on surfaces

Dedè, L.; Quarteroni, A.

MOX, Dipartimento di Matematica "F. Brioschi"
Politecnico di Milano, Via Bonardi 9 - 20133 Milano (Italy)

mox@mate.polimi.it http://mox.polimi.it

Isogeometric Analysis for second order Partial Differential Equations on surfaces

Luca Dedè [1,*] and Alfio Quarteroni [1,2]

[1] CMCS – Chair of Modeling and Scientific Computing
MATHICSE – Mathematics Institute of Computational Science and Engineering
EPFL – Eć ole Polytechnique Fédérale de Lausanne
Station 8, Lausanne, CH–1015, Switzerland

[2] MOX – Modeling and Scientific Computing
Mathematics Department "F. Brioschi"
Politecnico di Milano
via Bonardi 9, Milano, 20133, Italy

January 22, 2013

Abstract

We consider the numerical solution of second order Partial Differential Equations (PDEs) on lower dimensional manifolds, specifically on surfaces in three dimensional spaces. For the spatial approximation, we consider Isogeometric Analysis which facilitates the encapsulation of the exact geometrical description of the manifold in the analysis when this is represented by B–splines or NURBS. Our analysis addresses linear, nonlinear, time dependent, and eigenvalues problems involving the Laplace–Beltrami operator on surfaces. Moreover, we propose a priori error estimates under h–refinement in the general case of second order PDEs on the lower dimensional manifolds. We highlight the accuracy and efficiency of Isogeometric Analysis with respect to the exactness of the geometrical representations of the surfaces.

Key words. Second order Partial Differential Equations; Manifolds; Surfaces; Laplace–Beltrami operator; Isogeometric Analysis; A priori error estimation.

[*]Corresponding author. E-mail: luca.dede@epfl.ch, Phone: +41 21 6930318, Fax: +41 21 6935510.

1 Introduction

In several instances, Partial Differential Equations (PDEs) are set up on on lower dimensional manifolds with respect to the hosting physical space, namely on surfaces in three dimensions or curves in two or three–dimensions ([1]). Applications include problems in Fluid Dynamics, Biology, Electromagnetism, and image processing as reported for example in [8, 32, 23, 43, 45]. In addition, PDEs on lower dimensional manifolds could be obtained as reduced mathematical formulations of PDEs defined in thin geometries, e.g. for plates and shells structures [50].

The numerical approximation of these PDEs generally requires the generation of an approximated geometry compatible with the analysis, as it is the case for the Finite Element method (see e.g. [15, 33, 42]). In particular, the approximation of the curvature of surfaces may significantly affect the total error associated to the numerical approximation. Typically, schemes based on the Finite Element method have been used for the approximation of PDEs on surfaces with particular emphasis in controlling and limiting the propagation of the errors associated to the discrete geometrical representation. With this aim, surface Finite Element methods [22, 24] and geometrically consistent Finite Element mesh adaptations [9, 38] have been considered. As alternatives, approaches based on the implicit or immersed surfaces have been proposed, namely based on level set formulations [5, 23] or diffuse interfaces strategies [43]. Still, for a broad range of geometries (surfaces) of practical interest, the above mentioned approaches are not error free in the geometrical representation.

As alternative to these approaches, in this paper we propose numerical approximation of PDEs on lower dimensional manifolds by means of Isogeometric Analysis. Our approach is motivated by the fact that a broad range of geometries of practical interest are exactly represented by B–splines or NURBS ([40]).

Isogeometric Analysis is an approximation method for PDEs based on the isoparametric concept for which the same basis functions used for the geometrical representation are then also used for the numerical approximations of the PDEs [18, 34]. Typically, B–splines or NURBS geometrical representations are considered for Isogeometric Analysis, even if, more recently, T–splines ([47]) have been successfully utilized. Since NURBS are the golden standard in Computer Aided Design (CAD) technology, the use of Isogeometric Analysis facilitates the encapsulation of the exact geometrical representation in the analysis and simplifies the establishment of direct communications between design and numerical approximation of the PDEs. Moreover, NURBS–based Isogeometric Analysis possesses several advantages besides the geometrical considerations, especially in terms of smoothness of the basis functions and accuracy properties [2, 4, 28]. Nowadays, Isogeometric Analysis have been successfully used in a broad range of applications in computational mechanics and optimization, see e.g. [3, 18, 20, 31, 37]. In particular, Isogeometric Analysis have been considered for solving shell problems, as e.g. in [6], and, more recently, Isogeometric Analysis in the framework of the Boundary Element method ([52]) has been used to take advantage of the exact geometrical representation of surfaces [46].

In this work we provide for the first time a general formulation of the numerical approximation of second order PDEs defined on lower dimensional manifolds described by NURBS, specifically surfaces, by means of Isogeometric Analysis. We discuss the representation of the manifolds in a general framework by means of geometrical mappings from the parameter space to the physical domain; consequently, in view of the use of Isogeometric Analysis based on the Galerkin method ([42]), we recast the weak forms of the problems and the spatial differential operators in the parameter space. We provide a priori error estimates under h–refinement for the numerical approximation

by means of Isogeometric Analysis, thus extending the results of [2] and [4] to the case of the second order PDEs on lower dimensional manifolds; with this aim, an interpolation error estimate for the NURBS space on the manifold is proposed. We show the accuracy and efficiency of the method by solving several PDEs endowed with the Laplace–Beltrami spatial operator on surfaces. In particular, as few remarkable instances, we address the numerical solution of the Laplace–Beltrami problem, the eigenvalue problem, a time dependent linear advection–diffusion equation, and the Cahn–Allen phase transition equation ([11, 29]). For both the Laplace–Beltrami and the eigenvalue problems we compare the convergence rates of the errors obtained by means of Isogeometric Analysis with those expected from the a priori error estimates and we highlight the advantages of exactly representing the geometries at the coarsest level of discretization.

This work is organized as follows. In Sec. 2 we discuss the representation of lower dimensional manifolds by NURBS and the role of the parametrization in the definition of geometrical mappings. In Sec. 3 we consider the PDEs on the manifolds for problems involving the second order Laplace–Beltrami spatial operator. In Sec. 4 we discuss the numerical approximation schemes, specifically Isogeometric Analysis for the spatial approximation; for the time dependent problems, the generalized–α method ([14]) is considered and a SUPG stabilization scheme ([10]) is presented because of its suitability to treat advection dominated problems. In Sec. 5 we provide the interpolation error and a priori error estimates for h–refined NURBS "meshes". In Sec. 6 we report and discuss the numerical results for PDEs on surfaces. Final considerations are reported in the Conclusions.

2 Manifolds represented by NURBS

In this section we introduce in an abstract setting lower dimensional manifolds in the physical space, e.g. curves and surfaces, represented by suitable geometrical mappings. We recall the definition of generic functions and their derivatives on the manifold and we express them in terms of the parametric coordinates upon which the geometrical mapping is built. Finally, we specifically select manifolds defined by B–splines and NURBS and we briefly recall the basics of these geometrical representations.

2.1 Manifolds and geometrical mapping

Let us consider a generic (Riemannian) manifold, say $\Omega \subset \mathbb{R}^d$ with $d \geq 1$, defined in the physical space $\mathbb{R}^d$ [1]. Let us assume that the manifold is obtained by means of a geometrical mapping from a parameter space, say $\mathbb{R}^\kappa$, into the physical space $\mathbb{R}^d$, with $d \geq \kappa \geq 1$. If $d > \kappa$ the manifold is lower dimensional with respect to the physical space. More precisely, given a parameter domain, say $\widehat{\Omega} \subset \mathbb{R}^\kappa$, and a vector–valued independent variable $\boldsymbol{\xi} = (\xi_1, \ldots, \xi_\kappa) \in \mathbb{R}^\kappa$, the manifold $\Omega \subset \mathbb{R}^d$ is defined by means of the geometrical mapping:

$$\mathbf{x} \ : \ \widehat{\Omega} \to \mathbb{R}^d, \qquad \boldsymbol{\xi} \to \mathbf{x}(\boldsymbol{\xi}). \tag{2.1}$$

For example, if $d = 3$ and $\kappa = 1$, the manifold Ω represents a curve in $\mathbb{R}^3$, while if $\kappa = 2$, Ω is a surface in $\mathbb{R}^3$. Specifically, we consider compact, connected, and oriented manifolds Ω defined from parameter domains $\widehat{\Omega}$ of finite, positive measure with respect to the topology of $\mathbb{R}^\kappa$ ($0 < |\widehat{\Omega}| < +\infty$).

For the mapping (2.1), we define its Jacobian:

$$\widehat{\mathrm{F}} \ : \ \widehat{\Omega} \to \mathbb{R}^{d\times\kappa}, \qquad \boldsymbol{\xi} \to \widehat{\mathrm{F}}(\boldsymbol{\xi}), \qquad \widehat{\mathrm{F}}_{i,\alpha}(\boldsymbol{\xi}) := \frac{\partial \mathrm{x}_i}{\partial \xi_\alpha}(\boldsymbol{\xi}) \qquad i = 1, \ldots, d, \ \alpha = 1, \ldots, \kappa. \tag{2.2}$$

We also introduce the first fundamental form of the mapping:

$$\widehat{\mathrm{G}} \ : \ \widehat{\Omega} \to \mathbb{R}^{\kappa\times\kappa}, \qquad \boldsymbol{\xi} \to \widehat{\mathrm{G}}(\boldsymbol{\xi}), \qquad \widehat{\mathrm{G}}(\boldsymbol{\xi}) := \left(\widehat{\mathrm{F}}(\boldsymbol{\xi})\right)^T \widehat{\mathrm{F}}(\boldsymbol{\xi}) \tag{2.3}$$

and finally its determinant:

$$\widehat{g} \ : \ \widehat{\Omega} \to \mathbb{R}, \qquad \boldsymbol{\xi} \to \widehat{g}(\boldsymbol{\xi}), \qquad \widehat{g}(\boldsymbol{\xi}) := \sqrt{\det\left(\widehat{\mathrm{G}}(\boldsymbol{\xi})\right)}. \tag{2.4}$$

We observe that in the case for which $\kappa = d$, then $\widehat{\mathrm{F}}(\boldsymbol{\xi}) \in \mathbb{R}^{d\times d}$ and $\widehat{g}(\boldsymbol{\xi}) \equiv \det\left(\widehat{\mathrm{F}}(\boldsymbol{\xi})\right)$ (when positive). We assume that the geometrical mapping (2.1) is "sufficiently" smooth, e.g. $C^1(\widehat{\Omega})$, and invertible *a.e.* in $\widehat{\Omega}$. Notice that we allow the mapping to be locally not invertible in subdomains Q of Ω with zero measure in the topology of $\mathbb{R}^\kappa$; specifically, we require that $\widehat{g}(\boldsymbol{\xi}) > 0$ *a.e.* in $\widehat{\Omega}$ with $\widehat{g}(\boldsymbol{\xi}) = 0$ for $\boldsymbol{\xi} \in \widehat{Q} \subset \widehat{\Omega}$ only if $\mathrm{meas}\left(\widehat{Q}\right) \equiv 0$, where $\widehat{Q}$ is the subdomain of $\widehat{\Omega}$ mapping the subdomain Q of Ω.

Finally, in view of the derivation of the a priori error estimate in Sec. 5, we introduce, following Eqs. (2.2), (2.3), and (2.4), the Jacobian, the first fundamental form of the mapping, and its determinant in the manifold Ω as, respectively:

$$\mathrm{F} \ : \ \Omega \to \mathbb{R}^{d\times\kappa}, \qquad \mathbf{x} \to \mathrm{F}(\mathbf{x}), \qquad \mathrm{F}(\mathbf{x}) := \widehat{\mathrm{F}}(\boldsymbol{\xi}) \circ \mathbf{x}^{-1}(\boldsymbol{\xi}), \tag{2.5}$$

$$\mathrm{G} \ : \ \Omega \to \mathbb{R}^{\kappa\times\kappa}, \qquad \mathbf{x} \to \mathrm{G}(\mathbf{x}), \qquad \mathrm{G}(\mathbf{x}) := \widehat{\mathrm{G}}(\boldsymbol{\xi}) \circ \mathbf{x}^{-1}(\boldsymbol{\xi}), \tag{2.6}$$

$$g \ : \ \Omega \to \mathbb{R}, \qquad \mathbf{x} \to g(\mathbf{x}), \qquad g(\mathbf{x}) := \widehat{g}(\boldsymbol{\xi}) \circ \mathbf{x}^{-1}(\boldsymbol{\xi}). \tag{2.7}$$

where we used the geometrical mapping (2.1).

2.2 Functions and differential operators on manifolds

Let assume that a "sufficiently" regular function is defined on the manifold Ω, e.g. $\phi \in C^0(\Omega)$ for all $\mathbf{x} \in \Omega$; then, since we consider invertible geometrical mappings, we can write:

$$\phi(\mathbf{x}) = \widehat{\phi}(\boldsymbol{\xi}) \circ \mathbf{x}^{-1}(\boldsymbol{\xi}), \tag{2.8}$$

where $\widehat{\phi}(\boldsymbol{\xi}) := \phi\left(\mathbf{x}(\boldsymbol{\xi})\right)$. Moreover, we define the gradient on the manifold Ω of the function $\phi \in C^1(\Omega)$, say $\nabla_\Omega \phi \in \mathbb{R}^d$, as the projection of the gradient operator associated to the physical space onto the manifold. With this aim, we introduce the smooth prolongation of the function $\phi(\mathbf{x})$ from $\widehat{\Omega}$ into a tubular region in $\mathbb{R}^d$ containing $\widehat{\Omega}$ [9, 21], say $\widetilde{\phi}(\mathbf{x})$, and the projector tensor $\mathrm{P}(\mathbf{x}) \in \mathbb{R}^{d\times d}$:

$$\mathrm{P}(\mathbf{x}) := I - \mathbf{n}_\Omega(\mathbf{x}) \otimes \mathbf{n}_\Omega(\mathbf{x}) \qquad \text{for } \mathbf{x} \in \Omega, \tag{2.9}$$

with the unit vector $\mathbf{n}_\Omega(\mathbf{x})$ normal to the manifold Ω in $\mathbb{R}^d$ and I the identity tensor in $\mathbb{R}^{d\times d}$; in this manner, we have:

$$\nabla_\Omega \phi(\mathbf{x}) := \left[\mathrm{P}(\mathbf{x})\, \nabla \widetilde{\phi}(\mathbf{x})\right] \qquad \text{for } \mathbf{x} \in \Omega. \tag{2.10}$$

For example, for a curve in $\mathbb{R}^d$ we have $\nabla_\Omega \phi(\mathbf{x}) = \left(\nabla \widetilde{\phi}(\mathbf{x}) \cdot \mathbf{t}_\Omega(\mathbf{x})\right) \mathbf{t}_\Omega(\mathbf{x})$, where $\mathbf{t}_\Omega(\mathbf{x})$ is the unit tangent vector to the curve, while for a surface in $\mathbb{R}^d$, we obtain that $\nabla_\Omega \phi(\mathbf{x}) = \nabla \widetilde{\phi}(\mathbf{x}) - \left(\nabla \widetilde{\phi}(\mathbf{x}) \cdot \mathbf{n}_\Omega(\mathbf{x})\right) \mathbf{n}_\Omega(\mathbf{x})$[1]. Finally, we introduce the Laplace–Beltrami operator associated to the

[1] Notice that for a surface in $\mathbb{R}^3$ the unit normal vector $\mathbf{n}_\Omega(\mathbf{x})$ is obtained by mapping $\widehat{\mathbf{n}}_\Omega(\boldsymbol{\xi}) := \dfrac{\widehat{\mathbf{t}}_{\Omega,1}(\boldsymbol{\xi}) \times \widehat{\mathbf{t}}_{\Omega,2}(\boldsymbol{\xi})}{\|\widehat{\mathbf{t}}_{\Omega,1}(\boldsymbol{\xi}) \times \widehat{\mathbf{t}}_{\Omega,2}(\boldsymbol{\xi})\|}$ with $\widehat{\mathbf{t}}_{\Omega,\alpha}(\boldsymbol{\xi}) := \dfrac{\partial \mathbf{x}}{\partial \xi_\alpha}(\boldsymbol{\xi})$ for $\alpha = 1, 2$.

manifold Ω for a function $\phi \in C^2(\Omega)$ as:

$$\Delta_\Omega \phi(\mathbf{x}) := \nabla_\Omega \cdot (\nabla_\Omega \phi(\mathbf{x})) \,, \tag{2.11}$$

where the divergence operator $\nabla_\Omega \cdot$ is defined as $\nabla_\Omega \cdot \mathbf{v}(\mathbf{x}) = \text{trace}\,[\nabla_\Omega \mathbf{v}(\mathbf{x})]$ for all $\mathbf{v} \in \left[C^1(\Omega)\right]^d$. By using the notation of Eq. (2.10), we obtain for the Laplace–Beltrami operator:

$$\Delta_\Omega \phi(\mathbf{x}) = \text{trace}\left[\mathrm{P}(\mathbf{x})\, \nabla^2 \widetilde{\phi}(\mathbf{x})\, \mathrm{P}(\mathbf{x})\right] \qquad \text{for } \mathbf{x} \in \Omega, \tag{2.12}$$

where $\nabla^2 \cdot$ indicates the Hessian operator such that $\left(\nabla^2 \widetilde{\phi}(\mathbf{x})\right)_{i,j} := \dfrac{\partial^2 \widetilde{\phi}}{\partial \mathrm{x}_i \partial \mathrm{x}_j}(\mathbf{x})$ for $i, j = 1, \ldots, d$.

By using the geometrical mapping (2.1), the gradient on the manifold (2.10) can be rewritten as:

$$\nabla_\Omega \phi(\mathbf{x}) = \left[\widehat{\mathrm{F}}(\boldsymbol{\xi})\, \widehat{\mathrm{G}}^{-1}(\boldsymbol{\xi}) \widehat{\nabla} \widehat{\phi}(\boldsymbol{\xi})\right] \circ \mathbf{x}^{-1}(\boldsymbol{\xi}), \tag{2.13}$$

where $\widehat{\nabla}\widehat{\phi} \;:\; \widehat{\Omega} \to \mathbb{R}^\kappa$ is the gradient operator in the parameter space. Similarly, for the Laplace–Beltrami operator of Eq. (2.11), we have ([1]):

$$\Delta_\Omega \phi(\mathbf{x}) = \left[\frac{1}{\widehat{g}(\boldsymbol{\xi})}\, \widehat{\nabla} \cdot \left(\widehat{g}(\boldsymbol{\xi})\, \widehat{\mathrm{G}}^{-1}(\boldsymbol{\xi})\, \widehat{\nabla} \widehat{\phi}(\boldsymbol{\xi})\right)\right] \circ \mathbf{x}^{-1}(\boldsymbol{\xi}). \tag{2.14}$$

Finally, in view of the definitions of integrals in the weak form of the PDEs, the differential $d\mathbf{x}$ (or $d\Omega$) can be written as $d\mathbf{x} = \widehat{g}(\boldsymbol{\xi})\, d\boldsymbol{\xi}$ (or $d\Omega = \widehat{g}(\boldsymbol{\xi})\, d\widehat{\Omega}$).

2.3 Geometrical mapping by NURBS

We assume that the geometrical mapping introduced in Eq. (2.1) defines a manifold Ω represented by either B–splines or NURBS; for a detailed description we refer the reader to [40]. We observe that in the framework of Isogeometric Analysis, the choice of T–splines [47] represents a valid alternative and generalization.

The geometrical mapping (2.1) represented in terms of NURBS reads:

$$\mathbf{x}(\boldsymbol{\xi}) = \sum_{i=1}^{n_{bf}} \widehat{R}_i(\boldsymbol{\xi})\, \mathbf{P}_i, \tag{2.15}$$

where $\widehat{R}_i(\boldsymbol{\xi})$ are the NURBS basis functions defined in the parameter domain $\widehat{\Omega}$ and $\mathbf{P}_i \in \mathbb{R}^d$ are the control points in the physical space for $i = 1, \ldots, n_{bf}$. The NURBS basis functions $\widehat{R}_i(\boldsymbol{\xi})$ are defined from B–splines basis functions $\widehat{N}_i(\boldsymbol{\xi})$ and weights $w_i \in \mathbb{R}$ as:

$$\widehat{R}_i(\boldsymbol{\xi}) := \frac{w_i}{\displaystyle\sum_{i'=1}^{n_{bf}} w_{i'}\, \widehat{N}_{i'}(\boldsymbol{\xi})}\, \widehat{N}_i(\boldsymbol{\xi}) \qquad \text{for } i = 1, \ldots, n_{bf}; \tag{2.16}$$

we observe that B–splines geometries in $\mathbb{R}^d$ can be seen as a particular case of NURBS with weights equal to the unity[2]. The (multivariate) B–splines basis functions $\widehat{N}_i(\boldsymbol{\xi})$ are obtained by tensor product rule of univariate B–splines basis functions, say $\widehat{N}_{\alpha,i}(\xi_\alpha)$ for $i = 1, \ldots, n_{bf,\alpha}$, where

[2]NURBS are obtained by projective transformations of B–splines defined in the physical space $\mathbb{R}^{d+1}$.

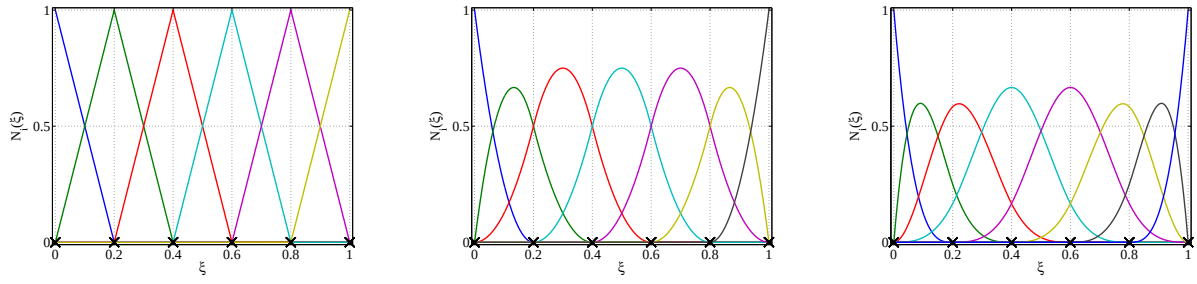

Figure 1: Univariate, globally C^{p-1}–continuous, B–splines basis functions $\left\{\widehat{N}_i(\xi)\right\}_{i=1}^{n}$ of order $p = 1, 2$, and 3 obtained by the knot vectors $\Xi = \left\{\{0\}^{p+1}, \frac{1}{5}, \frac{2}{5}, \frac{3}{5}, \frac{4}{5}, \{1\}^{p+1}\right\}$, respectively; $\widehat{\Omega} = (0, 1)$.

$\alpha = 1, \ldots, \kappa$ indicates the parametric direction ξ_α in $\mathbb{R}^\kappa$ with $\boldsymbol{\xi} = (\xi_1, \ldots, \xi_\kappa)$ and $n_{bf} = \Pi_{\alpha=1}^{\kappa} n_{bf,\alpha}$. The univariate B–splines basis functions $\widehat{N}_{\alpha,i}(\xi_\alpha)$ are recursively built by using the Cox–de Boor recursion formula starting from a knot vector $\Xi_\alpha := \{\xi_{\alpha,j}\}_{j=1}^{n_{bf,\alpha}+p_\alpha+1}$ with $\xi_{\alpha,j} \in \mathbb{R}$ which, together with the polynomial order p_α, completely characterizes the properties of the basis functions. We indicate the minimum polynomial order of the basis functions as $p := \min_{\alpha=1,\ldots,\kappa} p_\alpha$; in several instances, $p_\alpha = p$ for all $\alpha = 1, \ldots, \kappa$.

For example, in Fig. 1 we report open–knot, univariate B–splines basis functions of order $p = 1, 2, 3$ obtained by the knot vectors $\Xi = \left\{\{0\}^{p+1}, \frac{1}{5}, \frac{2}{5}, \frac{3}{5}, \frac{4}{5}, \{1\}^{p+1}\right\}$, respectively; we remark that the basis functions are globally C^{p-1}–continuous in $\widehat{\Omega} = (0, 1)$ for this specific choice of the knot vector.

We observe that the parameter domain $\widehat{\Omega}$ is obtained by the knot vectors Ξ_α for $\alpha = 1, \ldots, \kappa$ as $\widehat{\Omega} = (\xi_{1,1}, \xi_{n_{bf,1}+p_1+1}) \times \cdots \times (\xi_{\kappa,1}, \xi_{n_{bf,\kappa}+p_\kappa+1})$, which defines a NURBS patch; by convention, we consider the case for which $\widehat{\Omega} = (0, 1)^\kappa$, i.e. $\xi_{\alpha,1} = 0$ and $\xi_{n_{bf,\alpha}+p_\alpha+1} = 1$ for all $\alpha = 1, \ldots, \kappa$. The tensor product of the knots also defines a partition of the parameter domain $\widehat{\Omega}$ into subdomains $\widehat{\Omega}_e$, for $e = 1, \ldots, n_{el}$, which we regard as "mesh" elements in the parameter domain, n_{el} being their number; the set of these elements, i.e. the "mesh" of the parameter domain, is denoted as $\widehat{\mathcal{T}}_h$. The geometrical mapping (2.15) of the elements $\widehat{\Omega}_e$ into the physical space defines the elements Ω_e for $e = 1, \ldots, n_{el}$ and, similarly, the corresponding "mesh" in the physical domain $\mathcal{T}_h$. In addition, we introduce the notation $\widetilde{\widehat{\Omega}}_e$ to denote the support extension of $\widehat{\Omega}_e$, i.e. the union of the supports of the basis functions $\widehat{R}_i(\boldsymbol{\xi})$ for $i = 1, \ldots, n_{bf}$ whose supports possesses an intersection with $\widehat{\Omega}_e$ of non zero measure in the topology of $\mathbb{R}^\kappa$ ([2]); the mapping of the support extension in the parameter domain $\widetilde{\widehat{\Omega}}_e$ into the physical space is denoted by $\widetilde{\Omega}_e$. We schematically depict these concepts in Fig. 2. Finally, we indicate with $\widehat{h}_e$ the characteristic size (diameter) of the element $\widehat{\Omega}_e$ and with $\widehat{h}$ the global "mesh" size $\widehat{h} := \max\left\{\widehat{h}_e \ : \ \widehat{\Omega}_e \in \widehat{\mathcal{T}}_h\right\}$; correspondingly, we define the characteristic size (diameter) of the element Ω_e in the physical domain from Sec. 2.2 as:

$$h_e := \|\widehat{F}\|_{L^\infty(\widehat{\Omega}_e)} \widehat{h}_e \qquad \forall e = 1, \ldots, n_{el} \tag{2.17}$$

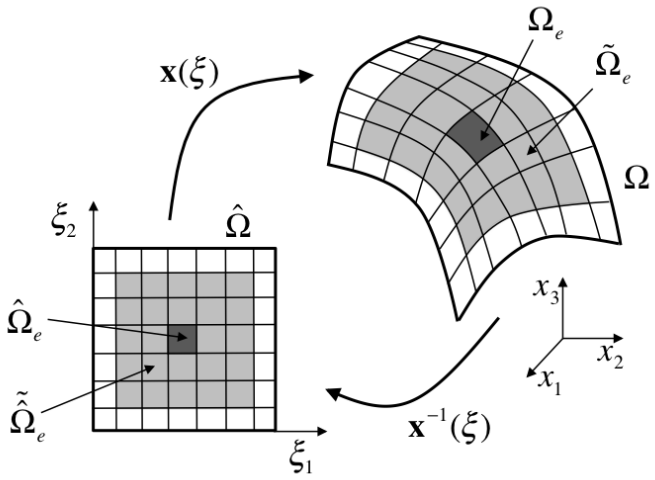

Figure 2: Illustration of a geometrical mapping $\mathbf{x}(\boldsymbol{\xi})$ from the parameter domain $\widehat{\Omega}$ into the manifold Ω (physical domain), a "mesh" element $\widehat{\Omega}_e$ and its support extension $\widetilde{\widehat{\Omega}}_e$ in the parameter domain, and the corresponding "mesh" element Ω_e and support extension $\widetilde{\Omega}_e$ into the physical space; the example refers to a B-splines or NURBS surface obtained with a basis of order $p = 2$ without internally repeated knots yielding $n_{el} = 49$ "mesh" elements.

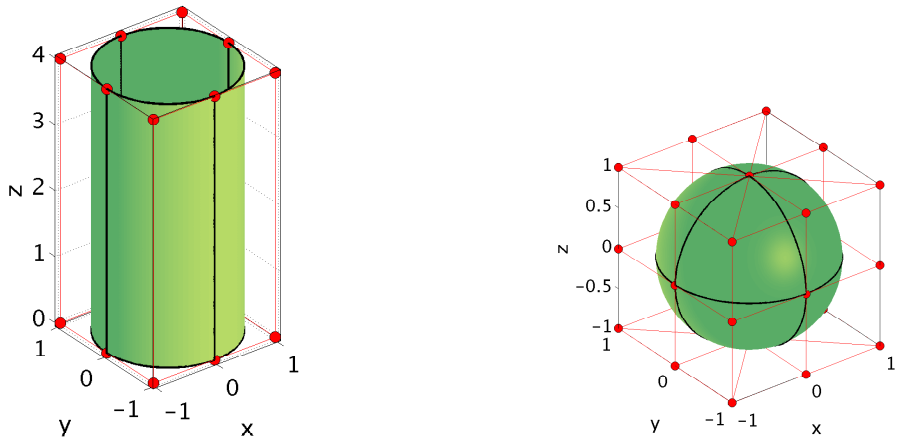

Figure 3: NURBS surfaces Ω in $\mathbb{R}^3$: cylindrical shell of radius 1 and height 4 (left) and spherical shell of radius 1 (right). The "mesh" elements are highlighted in black, the control net and control points $\{\mathbf{P}_i\}_{i=1}^{n_{bf}}$, in red.

and the global "mesh" size $h := \max\{h_e \ : \ \Omega_e \in \mathcal{T}_h\}$. We observe that the definition of h_e coincides with the one given in [2] for $\kappa = d$.

In Fig. 3 we report two examples of surfaces in $\mathbb{R}^3$ obtained by NURBS, a cylindrical and a spherical shell (we refer the reader to e.g. [18] and [40] for the construction of these geometries). We observe that both the geometries are exactly represented by NURBS at the coarsest level of discretization ($n_{el} = 4$ and 8 "mesh" elements and $n_{bf} = 18$ and 45 basis functions for the cylinder and the sphere, respectively).

In several circumstances, more complicated geometries can be generated by combining multiple NURBS patches.

3 PDEs on the manifold

With the aim of generality, we introduce a nonlinear parabolic PDE with second order spatial derivatives corresponding to the Laplace–Beltrami operator. Then, as particular cases of such general PDE, we present the equations we will address in this work, namely: an elliptic PDE, an eigenvalue problem, a time dependent advection–diffusion equation and the Cahn–Allen equation defined on the manifold. Then, in view of the numerical approximation, we rewrite the weak form of the equations in the parametric space by means of the geometrical mapping introduced in Sec. 2.

3.1 A nonlinear parabolic PDE with Laplace–Beltrami operator

Let us denote with $\Gamma = \partial\Omega$ the boundary of the manifold Ω. We say that Ω *possesses a boundary* if $\text{meas}(\Gamma) \neq 0$ in the topology of $\mathbb{R}^{\kappa-1}$; for example, by referring to Fig. 3 (left), the cylindrical shell has a boundary $\Gamma = \left\{\mathbf{x} = (\mathrm{x}, \mathrm{y}, \mathrm{z}) \in \mathbb{R}^3 \ : \ \mathrm{x}^2 + \mathrm{y}^2 = 1 \text{ and } \mathrm{z} = \{0, 4\}\right\}$, while the sphere does not posses a boundary ($\text{meas}(\Gamma) = 0$). If $\text{meas}(\Gamma) \neq 0$, then we can partition it into two non overlapping subdomains, say Γ_D and Γ_N, such that $\overline{\Gamma_D \cup \Gamma_N} \equiv \Gamma$ and $\overset{\circ}{\Gamma}_D \cap \overset{\circ}{\Gamma}_N = \emptyset$.

For the sake of simplicity and unless when necessary for clarity, we will omit from here on the explicit dependence of the functions defined in the physical space $\mathbb{R}^d$ on the spatial variable $\mathbf{x}$ and, similarly, for the functions in the parameter space $\mathbb{R}^\kappa$, the explicit dependence on the independent variable $\boldsymbol{\xi}$.

By recalling the definition of the Laplace–Beltrami operator (2.11), we assume the following expression for the time dependent nonlinear parabolic PDE, where $u(t)$ represents its solution:

$$\begin{aligned}
&\nu \frac{\partial u}{\partial t}(t) - \mu \Delta_\Omega u(t) + \mathbf{V} \cdot \nabla_\Omega u(t) + \sigma\left(u(t)\right) = f && \text{in } \Omega \times (0,T), \\
&u(t) = \gamma && \text{on } \Gamma_D \times (0,T), \\
&\mu \nabla_\Omega u(t) \cdot \mathbf{n}_\Gamma = 0 && \text{on } \Gamma_N \times (0,T), \\
&u(0) = u_{in} && \text{in } \Omega \times \{0\},
\end{aligned} \tag{3.1}$$

where $T > 0$ is the final time and $\mathbf{n}_\Gamma$ is the unit vector normal to the boundary Γ (note that $\mathbf{n}_\Gamma \cdot \mathbf{n}_\Omega = 0$ for all $\mathbf{x} \in \Gamma$). For simplicity, the coefficients $\nu \geq 0$ and $\mu > 0$ are assumed as constants in $\mathbb{R}$, the advection field $\mathbf{V} \in [L^\infty(\Omega)]^d$ is such that $\mathbf{V} \cdot \mathbf{n}_\Omega = 0$, $\nabla_\Omega \cdot \mathbf{V} \in L^2(\Omega)$ and $\nabla_\Omega \cdot \mathbf{V} = 0$ *a.e.* for $\mathbf{x} \in \Omega$, and the source term $f \in L^2(\Omega)$; the reaction term σ is assumed "sufficiently" regular, i.e. as $\sigma \in L^\infty(\Omega \times (0,T))$. Moreover, $\gamma \in H^{1/2}(\Gamma_D)$, and the initial condition $u_{in} \in L^2(\Omega)$; for the sake of simplicity, we assumed an homogeneous Neumann condition on Γ_N. We observe that, if the manifold Ω does not possesses a boundary ($\text{meas}(\Gamma) = 0$), the boundary conditions in Eq. (3.1) become meaningless and they should be replaced by other conditions on the solution $u(t)$ depending on the choice of the data (see Sec. 3.2).

In view of the weak form of the problem (3.1), we introduce the affine manifold $\mathcal{V}_\gamma$ and the function space $\mathcal{V}$ as:

$$\mathcal{V}_\gamma := \left\{v \in H^1(\Omega) \ : \ v|_{\Gamma_D} = \gamma\right\}, \qquad \mathcal{V} := \left\{v \in H^1(\Omega) \ : \ v|_{\Gamma_D} = 0\right\}. \tag{3.2}$$

Moreover, we introduce the following forms and functionals:

$$\begin{aligned} a(v,w) &:= \int_\Omega \mu\, \nabla_\Omega v \cdot \nabla_\Omega w \, d\Omega, & b(v,w) &:= \int_\Omega v\, \mathbf{V} \cdot \nabla_\Omega w \, d\Omega, \\ c(w)(v) &:= \int_\Omega v\, \sigma(w)\, d\Omega, & m(v,w) &:= \int_\Omega v\, w \, d\Omega, \\ q(v) &:= \int_\Omega v\, f \, d\Omega, \end{aligned} \tag{3.3}$$

and the weak residual:

$$\begin{aligned} Res\,(w(t))\,(v) \;:=\; & q(v) - a(v(t),w(t)) - b(v,w(t)) \\ & -c(w(t))(v) - \nu\, m\left(v, \frac{\partial w}{\partial t}(t)\right), \end{aligned} \tag{3.4}$$

for any $v \in \mathcal{V}$, $w(t) \in \mathcal{V}_\gamma$, for all $t \in (0,T)$. Then, the weak form of problem (3.1) reads, for all $t \in (0,T)$:

$$\begin{aligned} &\text{find } u(t) \in \mathcal{V}_\gamma \;:\; Res\,(u(t))\,(v) = 0 \qquad \forall v \in \mathcal{V}, \\ &\text{with } u(0) = u_{in}. \end{aligned} \tag{3.5}$$

We shall assume that the above problem is well–posed; for example, we observe that for $\nu = 1$, $\mathbf{V} = \mathbf{0}$, and $\sigma(u(t)) = \sigma_0\, u(t)$ for some $\sigma_0 > 0$, under the regularity hypothesis on the other data, we have a unique solution $u \in L^2\left((0,T);\mathcal{V}_\gamma\right) \cap C^0\left((0,T);L^2(\Omega)\right)$ by using similar arguments of [42]. For further details see e.g. [17, 25, 26, 27].

With the aim of writing problem (3.5) in the parameter space, we recall the mapping of the data based on Eqs. (2.1) and (2.8). In particular, we have: $\widehat{\mathbf{V}}(\boldsymbol{\xi}) := \mathbf{V}(\mathbf{x}(\boldsymbol{\xi}))$, $\widehat{f}(\boldsymbol{\xi}) := f(\mathbf{x}(\xi))$, $\widehat{\gamma}(\boldsymbol{\xi}) := \gamma(\mathbf{x}(\boldsymbol{\xi}))$, and $\widehat{u}_{in}(\boldsymbol{\xi}) := u_{in}(\mathbf{x}(\xi))$; we notice that $\widehat{\sigma}(\cdot) \equiv \sigma(\cdot)$. Moreover, we introduce the affine manifold $\widehat{\mathcal{V}}_\gamma$ and the function space $\widehat{\mathcal{V}}$ as:

$$\widehat{\mathcal{V}}_\gamma := \left\{\widehat{v} \in H^1(\widehat{\Omega}) \;:\; \widehat{v}|_{\widehat{\Gamma}_D} = \widehat{\gamma}\right\}, \qquad \widehat{\mathcal{V}} := \left\{\widehat{v} \in H^1(\widehat{\Omega}) \;:\; \widehat{v}|_{\widehat{\Gamma}_D} = 0\right\}, \tag{3.6}$$

where, if $\mathrm{meas}\,(\Gamma) \neq 0$, $\widehat{\Gamma}_D := \left\{\boldsymbol{\xi} \in \partial\widehat{\Omega} \;:\; \mathbf{x}(\boldsymbol{\xi}) \in \Gamma_D\right\}$ and $\widehat{\Gamma}_N = \partial\widehat{\Omega}\backslash\widehat{\Gamma}_D$. Also, we introduce the following forms and functionals from Eqs. (2.8), (2.13) and (3.3):

$$\begin{aligned} \widehat{a}(\widehat{v},\widehat{w}) &:= \int_{\widehat{\Omega}} \mu\, \widehat{\nabla}\widehat{v} \cdot \left(\widehat{\mathrm{G}}^{-1}\, \widehat{\nabla}\widehat{w}\right) \widehat{g}\, d\widehat{\Omega}, & \widehat{b}(\widehat{v},\widehat{w}) &:= \int_{\widehat{\Omega}} \widehat{v}\, \widehat{\mathbf{V}} \cdot \left(\widehat{\mathrm{F}}\, \widehat{\mathrm{G}}^{-1}\, \widehat{\nabla} w\right) \widehat{g}\, d\widehat{\Omega}, \\ \widehat{c}(\widehat{w})(\widehat{v}) &:= \int_{\widehat{\Omega}} \widehat{v}\, \widehat{\sigma}(\widehat{w})\, \widehat{g}\, d\widehat{\Omega}, & \widehat{m}(\widehat{v},\widehat{w}) &:= \int_{\widehat{\Omega}} \widehat{v}\, \widehat{w}\, \widehat{g}\, d\widehat{\Omega}, \\ \widehat{q}(\widehat{v}) &:= \int_{\widehat{\Omega}} \widehat{v}\, \widehat{f}\, \widehat{g}\, d\widehat{\Omega}, \end{aligned} \tag{3.7}$$

and the weak residual:

$$\widehat{Res}\,(\widehat{w}(t))\,(\widehat{v}) := \widehat{q}(\widehat{v}) - \widehat{a}(\widehat{v},\widehat{w}(t)) - \widehat{b}(\widehat{v},\widehat{w}(t)) - \widehat{c}(\widehat{w}(t))(\widehat{v}) - \nu\, \widehat{m}\left(\widehat{v}, \frac{\partial \widehat{w}}{\partial t}(t)\right), \tag{3.8}$$

for any $\widehat{v} \in \widehat{\mathcal{V}}$, $\widehat{w}(t) \in \widehat{\mathcal{V}}_\gamma$, and for all $t \in (0,T)$. Finally, the weak form of the problem (3.5) in the parameter space reads, for all $t \in (0,T)$:

$$\begin{aligned} &\text{find } \widehat{u}(t) \in \widehat{\mathcal{V}}_\gamma \;:\; \widehat{Res}\,(\widehat{u}(t))\,(\widehat{v}) = 0 \qquad \forall \widehat{v} \in \widehat{\mathcal{V}}, \\ &\text{with } \widehat{u}(0) = \widehat{u}_{in}; \end{aligned} \tag{3.9}$$

we observe that, from Eq. (2.8), we have $u(\mathbf{x},t) = \widehat{u}(\boldsymbol{\xi},t) \circ \mathbf{x}^{-1}(\boldsymbol{\xi})$ and $\widehat{u}(\boldsymbol{\xi},t) = u(\mathbf{x}(\boldsymbol{\xi}),t)$ for all $t \in (0,T)$.

3.2 The Laplace–Beltrami equation

By referring to Eq. (3.1) and assuming the data and solution u as time independent, $\nu = 0$, $\mathbf{V} = \mathbf{0}$, and $\sigma = 0$, we obtain the Laplace–Beltrami problem:

$$\text{find } u \in \mathcal{V}_\gamma \ : \ a(v,u) = q(v) \qquad \forall v \in \mathcal{V}, \tag{3.10}$$

for some $\mu > 0$. We observe that, if the manifold Ω is not endowed with a boundary, then the Laplace–Beltrami problem (3.10) is ill–posed. For this reason, if $\text{meas}\,(\Gamma) = 0$, the solution space $\mathcal{V}_\gamma$ is replaced e.g. by the space $\mathcal{V}_0 := \left\{ v \in H^1(\Omega) \ : \ \displaystyle\int_\Omega v \, d\Omega = 0 \right\}$ (see e.g. [39]).

By recasting problem (3.10) in the parameter space, we obtain:

$$\text{find } \widehat{u} \in \widehat{\mathcal{V}}_\gamma \ : \ \widehat{a}(\widehat{v},\widehat{u}) = \widehat{q}(\widehat{v}) \qquad \forall \widehat{v} \in \widehat{\mathcal{V}}, \tag{3.11}$$

where we have used the notation introduced in Sec. 3.1.

3.3 The Laplace–Beltrami eigenvalue problem

From Eq. (3.1), by assuming that the data and solution u are time independent, and setting $\nu = 0$, $\mathbf{V} = \mathbf{0}$, and $\sigma(u) = -\lambda\, u$, assuming the parameter λ as unknown, we obtain the Laplace–Beltrami eigenvalue problem[3]:

$$\text{find } u \in \mathcal{V} \text{ and } \lambda \in \mathbb{R} \ : \ a(v,u) = \lambda\, m(v,u) \qquad \forall v \in \mathcal{V}; \tag{3.12}$$

specifically, we set $\mu = 1$. We observe that, since the problem is symmetric, the eigenvalues are real valued, i.e. $\lambda \in \mathbb{R}$, with $\lambda \geq 0$.

In the parameter space, Eq. (3.12) reads:

$$\text{find } \widehat{u} \in \widehat{\mathcal{V}} \text{ and } \lambda \in \mathbb{R} \ : \ \widehat{a}(\widehat{v},\widehat{u}) = \lambda\, \widehat{m}(\widehat{v},\widehat{u}) \qquad \forall \widehat{v} \in \widehat{\mathcal{V}}. \tag{3.13}$$

3.4 A time dependent linear advection–diffusion equation

By using the notation of Sec. 3.1, we introduce the parabolic linear advection–diffusion equation in the following weak form, for all $t \in (0,T)$:

$$\begin{aligned} &\text{find } u(t) \in \mathcal{V}_\gamma \ : \ m\left(v, \frac{\partial u}{\partial t}(t)\right) + a(v,u(t)) + b(v,u(t)) = q(v) \qquad \forall v \in \mathcal{V}, \\ &\text{with } u(0) = u_{in}, \end{aligned} \tag{3.14}$$

where we set $\sigma(u(t)) = 0$ and $\nu = 1$. In view of the numerical approximation, we introduce the following operators, say $\mathcal{L}(\cdot)$ and $\mathcal{L}_{adv}(\cdot)$, as:

$$\mathcal{L}(w(t)) := \frac{\partial w}{\partial t}(t) - \mu\, \Delta_\Omega w(t) + \mathbf{V} \cdot \nabla_\Omega w(t), \tag{3.15}$$

[3] For $\sigma(u) = -\lambda\, u$, the form $c(\cdot)(\cdot)$ in Eq. (3.3) reads $c(w)(v) = -\lambda\, m(v,u)$ for any $v(\mathbf{x})$, $w(t) \in \mathcal{V}$.

$$\mathcal{L}_{adv}(w(t)) := \mathbf{V} \cdot \nabla_\Omega w(t), \tag{3.16}$$

and the strong residual $\mathcal{R}(\cdot)$ in Ω as:

$$\mathcal{R}\left(w(t)\right) := f - \mathcal{L}(w(t)), \tag{3.17}$$

for all $w(t) \in H^2(\Omega)$ for any $t \in (0,T)$.

In the parameter space, Eq. (3.14) reads, for all $t \in (0,T)$:

$$\begin{aligned} &\text{find } \widehat{u}(t) \in \widehat{\mathcal{V}}_\gamma \ : \ \widehat{m}\left(\widehat{v}, \frac{\partial \widehat{u}}{\partial t}(t)\right) + \widehat{a}(\widehat{v}, \widehat{u}(t)) + \widehat{b}(\widehat{v}, \widehat{u}(t)) = \widehat{q}(\widehat{v}) \qquad \forall \widehat{v} \in \widehat{\mathcal{V}}, \\ &\text{with } \widehat{u}(0) = \widehat{u}_{in}, \end{aligned} \tag{3.18}$$

while the operators and the residual in Eqs. (3.15), (3.16), and (3.17) are:

$$\widehat{\mathcal{L}}(\widehat{w}(t)) := \frac{\partial \widehat{w}}{\partial t}(t) - \mu \frac{1}{\widehat{g}} \widehat{\nabla} \cdot \left(\widehat{g}\, \widehat{\mathrm{G}}^{-1}\, \widehat{\nabla} \widehat{w}(t)\right) + \widehat{\mathbf{V}} \cdot \left(\widehat{\mathrm{F}}\, \widehat{\mathrm{G}}^{-1}\, \widehat{\nabla} \widehat{w}(t)\right), \tag{3.19}$$

$$\widehat{\mathcal{L}}_{adv}(\widehat{w}(t)) := \widehat{\mathbf{V}} \cdot \left(\widehat{\mathrm{F}}\, \widehat{\mathrm{G}}^{-1}\, \widehat{\nabla} \widehat{w}(t)\right), \tag{3.20}$$

$$\widehat{\mathcal{R}}\left(\widehat{w}(t)\right) := \widehat{f} - \widehat{\mathcal{L}}(\widehat{w}(t)), \tag{3.21}$$

for all $\widehat{w}(t) \in H^2(\widehat{\Omega})$ for any $t \in (0,T)$.

3.5 The Cahn–Allen equation

By denoting with $u(t)$ the concentration of a component of a binary isothermal mixture, we describe its evolution in time by means of the Cahn–Allen equation, a nonlinear, time dependent PDE. For further details on the topic we refer the reader e.g. to [11, 12, 13, 29]. The Cahn–Allen equation in weak form reads, for all $t \in (0,T)$:

$$\begin{aligned} &\text{find } u(t) \in \mathcal{V} \ : \ m\left(v, \frac{\partial u}{\partial t}(t)\right) + a(v, u(t)) + c(u(t))(v) = 0 \qquad \forall v \in \mathcal{V}, \\ &\text{with } u(0) = u_{in}, \end{aligned} \tag{3.22}$$

where, with reference to Eq. (3.1), we choose $\sigma(u(t)) = \Psi_{c,u}(u(t)) = 2u(t)\,(u(t)-1)\,(2u(t)-1)$ (for which we have that $c(u(t))(v) = \displaystyle\int_\Omega v\, \Psi_{c,u}(u(t))\, d\Omega$), $\mathbf{V} = \mathbf{0}$, $\nu = 1$, and $f = 0$. Moreover, if $\mathrm{meas}\,(\Gamma) \neq 0$, we set $\Gamma_N \equiv \Gamma$ with $\Gamma_D = \emptyset$. The Cahn–Allen equation (3.22) represents the gradient flow in the $L^2(\Omega)$ norm of the following energy functional (total free energy) for isothermal binary mixtures on surfaces:

$$\widetilde{\Psi}(t) = \Psi(u(t)) := \int_\Omega \left(\Psi_c(u(t)) + \frac{1}{2}\,\mu\,|\nabla_\Omega u(t)|^2\right) d\Omega, \tag{3.23}$$

where $\Psi_c(\cdot)$ is the chemical energy, which, in this specific case, we have choosen as $\Psi_c(u(t)) = (u(t))^2\,(u(t)-1)^2$; the functional $\Psi_{c,u}(\cdot) = \sigma(\cdot)$ represents the chemical potential and is obtained as the Frechét derivative of $\Psi_c(\cdot)$ with respect to the variable $u(t)$. The free energy $\widetilde{\Psi}(t)$ represents a Liapunov functional since $\dfrac{d\widetilde{\Psi}}{dt}(t) \leq 0$ for all $t \in (0,T]$, being $\nabla_\Omega u(t) \cdot \widehat{\mathbf{n}}_\Gamma = 0$ on Γ.

In the parameter space, the Cahn–Allen equation reads, for all $t \in (0, T)$:

$$\begin{aligned} &\text{find } \widehat{u}(t) \in \widehat{\mathcal{V}} \ : \ \widetilde{m}\left(\widehat{v}, \frac{\partial \widehat{u}}{\partial t}(t)\right) + \widehat{a}(\widehat{v}, \widehat{u}(t)) + \widehat{c}(\widehat{u}(t))(\widehat{v}) = 0 \qquad \forall \widehat{v} \in \widehat{\mathcal{V}}, \\ &\text{with } \widehat{u}(0) = \widehat{u}_{in}, \end{aligned} \tag{3.24}$$

with the free energy:

$$\widetilde{\Psi}(t) = \widehat{\Psi}(u(t)) := \int_{\widehat{\Omega}} \left(\Psi_c(\widehat{u}(t)) + \frac{1}{2}\, \mu\, \widehat{\nabla} \widehat{u}(t) \cdot \left(\widehat{\mathrm{G}}^{-1}\, \widehat{\nabla} \widehat{u}(t) \right) \right) \widehat{g}\, d\widehat{\Omega}, \tag{3.25}$$

being $\widehat{\Psi}_c(\cdot) \equiv \Psi_c(\cdot)$.

4 Numerical approximation

In this section we describe the numerical approximation of the PDEs introduced in Sec. 3.1 and represented in compact form in Eq. (3.5). We discuss the approximation in a general setting, firstly for the spatial approximation by means of Isogeometric Analysis and then, for time discretization, the generalized–α method.

4.1 The spatial approximation: Isogeometric Analysis

For the spatial approximation of the general problem (3.5) we consider Isogeometric Analysis. In this section we briefly recall the basic notions of the approximation in the framework of the Galerkin method. For further details we refer the reader to [18, 34].

Isogeometric Analysis is a method for the spatial approximation of PDEs, based on the isoparametric concept for which the same basis used to represent the known geometry are then used to approximate the unknown solution of the PDEs. NURBS or B–splines geometries (computational domains) are represented by geometrical mappings in the form (2.15) from a parameter space to the physical space. By using the isogeometric paradigm, we can define functions in the parameter space in the form:

$$\widehat{u}_h(\boldsymbol{\xi}, t) := \sum_{i=1}^{n_{bf}} \widehat{R}_i(\boldsymbol{\xi})\, U_i(t), \tag{4.1}$$

where $\widehat{R}_i(\boldsymbol{\xi})$ are the NURBS (or B–splines) basis functions (see Eq. (2.16)) and $U_i(t) \in \mathbb{R}$ are the control variables (in fact, the problem unknowns) for $i = 1, \ldots, n_{bf}$, with n_{bf} the number of basis functions; for time dependent problems, the control variables $U_i(t)$ are time dependent. Since the geometrical mapping (2.15) is invertible (as discussed in Secs. 2.1 and 2.3)), we can indifferently refer to functions in the parameter space or in the physical one; from Eq. (2.8) we have $u_h(\mathbf{x}, t) = \widehat{u}_h(\boldsymbol{\xi}, t) \circ \mathbf{x}^{-1}(\boldsymbol{\xi})$. For this reason, unless than necessary for clarity, we will henceforth consider formulations in the parameter space.

From Eq. (4.1) we define the NURBS space on the parameter domain $\widehat{\Omega}$ (a single patch):

$$\widehat{\mathcal{N}}_h := \text{span} \left\{ \widehat{R}_i(\boldsymbol{\xi}) \right\}_{i=1}^{n_b f} \tag{4.2}$$

and, in virtue of the geometrical mapping (2.15), the corresponding NURBS space on the physical domain (the manifold) Ω:

$$\mathcal{N}_h := \text{span} \left\{ \widehat{R}_i(\boldsymbol{\xi}) \circ \mathbf{x}^{-1}(\boldsymbol{\xi}) \right\}_{i=1}^{n_b f}. \tag{4.3}$$

Then, we introduce the finite dimensional function spaces $\widehat{\mathcal{V}}_{\gamma,h} := \widehat{\mathcal{V}}_\gamma \cap \widehat{\mathcal{N}}_h$ and $\widehat{\mathcal{V}}_h := \widehat{\mathcal{V}} \cap \widehat{\mathcal{N}}_h$ from Eqs. (3.6) and (4.1); for simplicity, we assume that the data $\widehat{\gamma}$ belongs to the NURBS space $\widehat{\mathcal{N}}_h$. Similarly, by referring to the physical domain Ω, we introduce the function spaces $\mathcal{V}_{\gamma,h} := \mathcal{V}_\gamma \cap \mathcal{N}_h$ and $\mathcal{V}_h := \mathcal{V} \cap \mathcal{N}_h$.

The weak form of problem (3.9) approximated by Isogeometric Analysis reads, for all $t \in (0,T)$:

$$\begin{aligned} &\text{find } \widehat{u}_h(t) \in \widehat{\mathcal{V}}_{\gamma,h} \ : \ \widehat{Res}\left(\widehat{u}_h(t)\right)(\widehat{v}_h) = 0 \qquad \forall \widehat{v}_h \in \widehat{\mathcal{V}}_h, \\ &\text{with } \widehat{u}_h(0) = \widehat{u}_{in,h}, \end{aligned} \tag{4.4}$$

where $\widehat{u}_{in,h}$ is the $L^2(\Omega)$ projection of $\widehat{u}_{in}$ onto $\widehat{\mathcal{V}}_h$. The spatial approximation of the problems described in Secs. 3.2, 3.4, and 3.5 fit the general formulation of Eq. (4.4), while the eigenvalue problem (3.13) reads:

$$\text{find } \widehat{u}_h \in \widehat{\mathcal{V}}_h \text{ and } \lambda_h \in \mathbb{R} \ : \ \widehat{a}(\widehat{v}_h, \widehat{u}_h) = \lambda_h\, \widehat{m}(\widehat{v}_h, \widehat{u}_h) \qquad \forall \widehat{v}_h \in \widehat{\mathcal{V}}_h. \tag{4.5}$$

We remark that the function spaces $\widehat{\mathcal{V}}_{\gamma,h}$ and $\widehat{\mathcal{V}}_h$ can be "enriched" by means of h– or p–refinement of the geometric representation while identically preserving the geometrical mapping[4]. The refinements allow the improvement of the accuracy of the approximate solution, while still representing exactly the NURBS geometries defining the computational domain. A type of refinement called k–refinement and specific for NURBS basis functions can be eventually used to efficiently improve the accuracy by increasing the order p of the basis functions and their global continuity, say k, across the elements $\widehat{\Omega}_e$ in $\widehat{\Omega}$ while containing the number of basis functions n_{bf}. For further details we refer the reader to [2, 4, 18, 19, 34]. Specifically, in Sec. 5 we provide a priori error estimates for PDEs on manifolds for h–refined "meshes".

We remark that numerical integration is performed by means of a quadrature formula with $(p+1)^\kappa$ quadrature points in each element; a direct method ([41]) is considered for the solution of the linear system associated to Eq. (4.4).

4.2 The time discretization scheme

For the approximation of time dependent problems, we consider the generalized–α method, a predictor–multicorrector numerical scheme, which we briefly recall in this section; for further details see also e.g. [14, 36].

Let start by introducing a partition of the time interval $(0,T)$ into time steps $\{t_n\}_{n=0}^{n_{ts}}$, where $t_0 = 0$ and $t_{n_{ts}} = T$, with time steps $\Delta t_n := t_{n+1} - t_n$ for $n = 0, \ldots, t_{n_{ts}-1}$. Also, we define $\mathbf{U}(t) := \{U_i(t)\}_{i=1}^{n_{bf}}$, $\dot{\mathbf{U}}(t) := \left\{\dot{U}_i(t)\right\}_{i=1}^{n_{bf}}$, $\widehat{\mathbf{Res}}\left(\dot{\mathbf{U}}(t), \mathbf{U}(t)\right) := \left\{\widehat{Res}\left(\widehat{u}_h(t)\right)\left(\widehat{R}_i\right)\right\}_{i=1}^{n_{bf}}$ from Eq. (3.8), $\mathbf{U}_n := \mathbf{U}(t_n)$, and $\dot{\mathbf{U}}_n := \dot{\mathbf{U}}(t_n)$. By introducing the parameters α_m, α_f, and $\delta \in \mathbb{R}$, the generalized–α method consists in solving the following problem at the time step t_{n+1} given $\dot{\mathbf{U}}_n$ and $\mathbf{U}_n$:

$$\begin{aligned} &\text{find } \dot{\mathbf{U}}_{n+1}, \mathbf{U}_{n+1}, \dot{\mathbf{U}}_{n+\alpha_m}, \mathbf{U}_{n+\alpha_f} \ : \ \widehat{\mathbf{Res}}\left(\dot{\mathbf{U}}_{n+\alpha_m}, \mathbf{U}_{n+\alpha_f}\right) = \mathbf{0}, \\ &\text{with: } \mathbf{U}_{n+1} = \mathbf{U}_n + \Delta t_n \left((1-\delta)\,\dot{\mathbf{U}}_n + \delta\,\dot{\mathbf{U}}_{n+1}\right), \\ &\qquad \dot{\mathbf{U}}_{n+\alpha_m} = (1-\alpha_m)\,\dot{\mathbf{U}}_n + \alpha_m\,\dot{\mathbf{U}}_{n+1}, \qquad \mathbf{U}_{n+\alpha_f} = (1-\alpha_f)\,\mathbf{U}_n + \alpha_f\,\mathbf{U}_{n+1}. \end{aligned} \tag{4.6}$$

[4] The h– or p–refinements correspond to the mesh refinement and order elevation procedures of the Finite Element or Spectral methods.

The previous problem is solved iteratively with $\mathbf{U}_{n+1}$ obtained as $\mathbf{U}_{n+1,(j)}$ for some $j = 0, \dots, j_{max}$ (with $j_{max} > 1$). In particular, at the predictor stage ($j = 0$), we set:

$$\dot{\mathbf{U}}_{n+1,(0)} = \frac{\delta - 1}{\delta} \dot{\mathbf{U}}_n, \qquad \mathbf{U}_{n+1,(0)} = \mathbf{U}_n. \tag{4.7}$$

At the multicorrector stage, we repeat for $j = 1, \dots, j_{max}$ the following steps:

1. evaluate the variables:

$$\dot{\mathbf{U}}_{n+\alpha_m,(j)} = (1-\alpha_m)\, \dot{\mathbf{U}}_n + \alpha_m\, \dot{\mathbf{U}}_{n+1,(j-1)}, \qquad \mathbf{U}_{n+\alpha_f,(j)} = (1-\alpha_f)\, \mathbf{U}_n + \alpha_f\, \mathbf{U}_{n+1,(j-1)}; \tag{4.8}$$

2. assemble the residual vector and tangent matrix:

$$\begin{aligned} &\widehat{\mathbf{Res}}_{n+1,(j)} := \widehat{\mathbf{Res}}\left(\dot{\mathbf{U}}_{n+\alpha_m,(j)}, \mathbf{U}_{n+\alpha_f,(j)}\right), \\ &\widehat{\mathbf{K}}_{n+1,(j)} := \alpha_m \frac{\partial \widehat{\mathbf{Res}}\left(\dot{\mathbf{U}}_{n+\alpha_m,(j)}, \mathbf{U}_{n+\alpha_f,(j)}\right)}{\partial \dot{\mathbf{U}}_{n+\alpha_m}} + \alpha_f\, \delta\, \Delta t_n \frac{\partial \widehat{\mathbf{Res}}\left(\dot{\mathbf{U}}_{n+\alpha_m,(j)}, \mathbf{U}_{n+\alpha_f,(j)}\right)}{\partial \mathbf{U}_{n+\alpha_f}}; \end{aligned} \tag{4.9}$$

3. if, for a prescribed tolerance $tol_R > 0$, the criterion $\dfrac{\|\widehat{\mathbf{Res}}_{n+1,(j)}\|}{\|\widehat{\mathbf{Res}}_{n+1,(0)}\|} \leq tol_R$ is fulfilled, set $\dot{\mathbf{U}}_{n+1} = \dot{\mathbf{U}}_{n+1,(j-1)}$ and $\mathbf{U}_{n+1} = \mathbf{U}_{n+1,(j-1)}$ and terminate the procedure, otherwise continue;

4. solve the linear system:

$$\widehat{\mathbf{K}}_{n+1,(j)}\, \Delta\dot{\mathbf{U}}_{n+1,(j)} = -\widehat{\mathbf{Res}}_{n+1,(j)}; \tag{4.10}$$

5. update the variables:

$$\dot{\mathbf{U}}_{n+1,(j)} = \dot{\mathbf{U}}_{n+1,(j-1)} + \Delta\dot{\mathbf{U}}_{n+1,(j)}, \qquad \mathbf{U}_{n+1,(j)} = \mathbf{U}_{n+1,(j-1)} + \delta\, \Delta t_n\, \Delta\dot{\mathbf{U}}_{n+1,(j)}, \tag{4.11}$$

and return to step 1.

A family of second–order time accurate and unconditionally stable generalized–α methods for linear problems is obtained by choosing $\alpha_m = \dfrac{1}{2}\left(\dfrac{3-\rho_\infty}{1+\rho_\infty}\right)$, $\alpha_f = \delta = \dfrac{1}{1+\rho_\infty}$, where $\rho_\infty \in [0,1]$ governs high frequencies dissipation [33][5]; a typical choice is $\rho_\infty = 0.5$, see e.g. [20, 31, 37].

The time step Δt_n can be either fixed ($\Delta t_n = \Delta t_0$) or determined by an adaptive algorithm. In the latter case, we select an adaptive scheme based on the number of iterations of the multicorrector stage of the generalized–α method (see e.g. [31, 51]); in particular, based on numerical experience, we set $\Delta t_n = \Delta t_{n-1}\, \chi \sqrt{\dfrac{j}{j_{ref} + j_0}}$ for $n = 1, \dots, t_{n_{ts}-1}$ and an initial time step Δt_0, where $\chi = 1.2$, $j_{ref} = 2$, and $j_0 = 0.8$. As tolerance for the stopping criterion of the multicorrector stage we select $tol_R = 10^{-4}$.

[5] The parameter ρ_∞ represents the spectral radius of the amplification matrix of the system for $\Delta t_n \to \infty$.

4.3 SUPG stabilization for the advection–diffusion PDEs

Since we are interested in solving time dependent advection–diffusion equations in the transport dominated regime, we consider the numerical stabilization of the PDEs in lower dimensional manifolds. In particular, we consider a SUPG stabilization technique similar to the one proposed in [39] for PDEs on surfaces approximated by means of the Finite Element method.

The time dependent linear advection–diffusion problem (3.18) with SUPG stabilization ([10]) reads, for all $t \in (0,T)$:

$$\begin{aligned} &\text{find } \widehat{u}_h(t) \in \widehat{\mathcal{V}}_{\gamma,h} \ : \ \widehat{m}\left(\widehat{v}_h, \frac{\partial \widehat{u}_h}{\partial t}(t)\right) + \widehat{a}(\widehat{v}_h, \widehat{u}_h(t)) + \widehat{b}(\widehat{v}_h, \widehat{u}_h(t)) \\ &\qquad\qquad + \widehat{d}_h(\widehat{v}_h, \widehat{u}_h(t)) - \widehat{q}(\widehat{v}_h) = 0 \qquad \forall \widehat{v}_h \in \widehat{\mathcal{V}}_h, \\ &\text{with } \widehat{u}_h(0) = \widehat{u}_{in,h}, \end{aligned} \tag{4.12}$$

where the form $\widehat{d}_h(\cdot,\cdot)$ represents the SUPG stabilization term. By recalling the definitions (3.20) and (3.21), we define:

$$\widehat{d}_h(\widehat{v}_h, \widehat{w}_h(t)) := \sum_{e=1}^{n_{el}} \int_{\widehat{\Omega}_e} \tau_e \, \widehat{\mathcal{L}}_{adv}\,(\widehat{v}_h)\ \widehat{\mathcal{R}}(\widehat{w}_h(t))\, \widehat{g}\, d\widehat{\Omega}, \tag{4.13}$$

for all $\widehat{v}_h$ and $\widehat{w}_h(t) \in H^2(\widehat{\Omega}_e)$, with $e = 1, \ldots, n_{el}$, and $t \in (0,T)$; the stabilization parameter τ_e is assumed as piecewise constant over the elements $\widehat{\Omega}_e$[6]. We introduce the characteristic velocity $V_e := \|\widehat{\mathbf{V}}\|_{L^\infty(\widehat{\Omega}_e)}$, the constant c_p depending on the order p of the polynomial approximation[7], and the local Péclet number $\mathbb{P}e_e := \dfrac{V_e\, h_e}{2\mu}$. Following [30, 35, 48], we choose:

$$\tau_e := \frac{1}{2}\left[\frac{1}{\Delta t^2} + \left(\frac{V_e}{h_e}\right)^2 \left(1 + \left(\frac{c_p}{\mathbb{P}e_e}\right)^2\right)\right]^{-1/2}, \tag{4.14}$$

where h_e is the characteristic size (diameter) of the element Ω_e (2.17) and Δt is the time step for the time approximation; we will assume $c_p = p^2$. This choice of τ_e is obtained by locally approximating the operator $\widehat{\mathcal{L}}^{-1}(\cdot)$, by assuming the use of second order time schemes (as the generalized–α method), and by considering geometrical mappings of the elements Ω_e from parents domains $(-1,1)^\kappa$; the parameter τ_e assumes the same form in the parameter and physical spaces.

5 A priori error estimation on lower dimensional manifolds

We provide the a priori error estimates under h–refinement for the Laplace–Beltrami equation (3.10) and the Laplace–Beltrami eigenvalue problem (3.12) thus extending the results of [2] (and [4]) to the case of second order PDEs defined on lower dimensional manifolds. With this aim, we propose

[6] We notice that in the physical space we have, from Eqs. (3.16) and (3.17), $d_h(v_h, w_h(t)) := \sum_{e=1}^{n_{el}} \int_{\Omega_e} \tau_e\, \mathcal{L}_{adv}\,(v_h)\ \mathcal{R}(w_h(t))\ d\Omega$ for all v_h and $w_h(t) \in H^2(\Omega_e)$, with $e = 1, \ldots, n_{el}$, and $t \in (0,T)$.

[7] The constant c_p stems from an inverse inequality of the type $\|\Delta_\Omega v_h\|_{L^2(\Omega_e)} \leq \dfrac{c_p}{h_e}\, \|\nabla_\Omega v_h\|_{L^2(\Omega_e)}$ for all $v_h \in \mathcal{V}_h$ and $e = 1, \ldots, n_{el}$.

some preliminary estimates for the change of variables between the parameter and the physical domains and the interpolation error estimate for the NURBS space on the physical domain (the lower dimensional manifold); for simplicity, we limit to consider estimates up to the H^1 norm. We remark that, for the derivation of the error estimate, we follow the procedure and recall the results presented in [2].

5.1 The interpolation error estimate

Let us recall the notation of Secs. 2.1 and 2.3 regarding the geometrical mapping by NURBS and of Sec. 4.1 for the NURBS spaces. Moreover, we recall the definition of the H^1 semi–norm on the manifold $|\phi|_{H^1(\Omega)} := \left(\int_\Omega |\nabla_\Omega \phi|^2 \, d\Omega \right)^{1/2}$ from Eq. (2.10); the definition of high order semi–norms follows consequently. Similarly, the L^2 norm on the manifold reads: $\|\phi\|_{L^2(\Omega)} := \left(\int_\Omega |\phi|^2 \, d\Omega \right)^{1/2}$.

In analogy with [2] for the case $\kappa = d$, we provide the following preliminary results for functions defined on manifolds represented by NURBS.

Proposition 5.1. *Let us consider an integer $m = 0, 1$, the general "mesh" element in the parameter domain $\widehat{\Omega}_e \in \widehat{\mathcal{T}}_h$ and its corresponding "mesh" element on the manifold $\Omega_e \in \mathcal{T}_h$. We obtain for $\phi \in H^m(\Omega_e)$ and $\widehat{\phi} \in H^m(\widehat{\Omega}_e)$:*

$$|\widehat{\phi}|_{H^m(\widehat{\Omega}_e)} \leq \left\| \frac{1}{g} \right\|^{1/2}_{L^\infty(\Omega_e)} \sum_{j=0}^{m} \left[\left\| \widehat{F} \right\|^{j}_{L^\infty(\widehat{\Omega}_e)} |\phi|_{H^j(\Omega_e)} \right], \tag{5.1}$$

$$|\phi|_{H^m(\Omega_e)} \leq C_{shape} \, \|\widehat{g}\|^{1/2}_{L^\infty(\widehat{\Omega}_e)} \left\| \widehat{F} \right\|^{-m}_{L^\infty(\widehat{\Omega}_e)} \sum_{j=0}^{m} \left| \widehat{\phi} \right|_{H^j(\widehat{\Omega}_e)}, \tag{5.2}$$

where C_{shape} is a positive and dimensionless constant depending on the shape of the manifold Ω, but not its size [2].

Proof. We start by proving the result (5.1) for $m = 1$, the case $m = 0$ following similarly. From Eq. (2.13) and by observing that $\widehat{\nabla} \widehat{\phi}(\boldsymbol{\xi}) = \left(\widehat{F}(\boldsymbol{\xi}) \right)^T \nabla_\Omega \phi(\mathbf{x}(\boldsymbol{\xi}))$, we obtain (in analogy with [16]):

$$\left| \widehat{\nabla} \widehat{\phi}(\boldsymbol{\xi}) \right| \leq \left| \widehat{F}(\boldsymbol{\xi}) \right| \, |\nabla_\Omega \phi(\mathbf{x})| \,, \tag{5.3}$$

for all $\boldsymbol{\xi} \in \widehat{\Omega}_e$ with $\mathbf{x} = \mathbf{x}(\boldsymbol{\xi}) \in \Omega_e$ (in Euclidean norm). By elevating the terms of the inequality to the square, integrating over the "mesh" element $\widehat{\Omega}_e$, and recalling the definition of H^1 semi–norm, we obtain:

$$\left| \widehat{\phi} \right|^2_{H^1(\widehat{\Omega}_e)} \leq \left\| \widehat{F} \right\|^2_{L^\infty(\widehat{\Omega}_e)} \int_{\widehat{\Omega}_e} |\nabla_\Omega \phi|^2 \, d\widehat{\Omega}_e. \tag{5.4}$$

Since $\displaystyle\int_{\widehat{\Omega}_e} |\nabla_\Omega \phi|^2 \, d\widehat{\Omega}_e = \int_{\Omega_e} |\nabla_\Omega \phi|^2 \, \frac{1}{g} \, d\Omega_e$ from Eq. (2.7), we obtain:

$$\left| \widehat{\phi} \right|^2_{H^1(\widehat{\Omega}_e)} \leq \left\| \frac{1}{g} \right\|_{L^\infty(\Omega_e)} \left\| \widehat{F} \right\|^2_{L^\infty(\widehat{\Omega}_e)} \int_{\Omega_e} |\nabla_\Omega \phi|^2 \, d\Omega_e, \tag{5.5}$$

from which the result (5.1) follows.

We proceed in a similar manner for the result (5.2). From Eqs. (2.5), (2.6), and (2.13) we have:

$$|\nabla_\Omega \phi(\mathbf{x})| \leq \left|F(\mathbf{x})\, G^{-1}(\mathbf{x})\right| \left|\widehat{\nabla}\widehat{\phi}(\boldsymbol{\xi})\right|, \tag{5.6}$$

for all $\mathbf{x} \in \Omega_e$ with $\boldsymbol{\xi} = \mathbf{x}^{-1}(\boldsymbol{\xi}) \in \widehat{\Omega}_e$ (in Euclidean norm). We obtain that:

$$|\phi|^2_{H^1(\Omega_e)} \leq \left\|F\, G^{-1}\right\|^2_{L^\infty(\Omega_e)} \int_{\Omega_e} \left|\widehat{\nabla}\widehat{\phi}\right|^2 d\Omega_e. \tag{5.7}$$

and, since $\displaystyle\int_{\Omega_e} \left|\widehat{\nabla}\widehat{\phi}\right|^2 d\Omega_e = \int_{\widehat{\Omega}_e} \left|\widehat{\nabla}\widehat{\phi}\right|^2 \widehat{g}\, d\widehat{\Omega}_e$, we have:

$$|\phi|^2_{H^1(\Omega_e)} \leq \|\widehat{g}\|_{L^\infty(\widehat{\Omega}_e)} \left\|F\, G^{-1}\right\|^2_{L^\infty(\Omega_e)} \int_{\widehat{\Omega}_e} \left|\widehat{\nabla}\widehat{\phi}\right|^2 d\widehat{\Omega}_e, \tag{5.8}$$

from which we deduce that:

$$|\phi|_{H^1(\Omega_e)} \leq \|\widehat{g}\|^{1/2}_{L^\infty(\widehat{\Omega}_e)} \left\|F\, G^{-1}\right\|_{L^\infty(\Omega_e)} |\phi|_{H^j(\widehat{\Omega}_e)}. \tag{5.9}$$

In analogy with [2] we introduce from Eqs. (2.1) and (2.2) the locally rescaled geometrical mapping:

$$\breve{\mathbf{x}} \;:\; \widehat{\Omega}_e \to \breve{\Omega}_e, \qquad \boldsymbol{\xi} \to \breve{\mathbf{x}}(\boldsymbol{\xi}), \qquad \breve{\mathbf{x}}(\boldsymbol{\xi}) = \mathbf{x}(\boldsymbol{\xi}) \left\|\widehat{F}\right\|^{-1}_{L^\infty(\widehat{\Omega}_e)}, \tag{5.10}$$

for all $\widehat{\Omega}_e \in \widehat{\mathcal{T}}_h$, where $\breve{\Omega}_e$ belongs to the physical space; correspondingly, we define its Jacobian:

$$\widehat{\breve{F}} \;:\; \widehat{\Omega}_e \to \mathbb{R}^{d\times\kappa}, \qquad \boldsymbol{\xi} \to \widehat{\breve{F}}(\boldsymbol{\xi}), \qquad \widehat{\breve{F}}_{i,\alpha}(\boldsymbol{\xi}) := \frac{\partial \breve{\mathrm{x}}_i}{\partial \xi_\alpha}(\boldsymbol{\xi}) \qquad i = 1,\ldots,d,\ \alpha = 1,\ldots,\kappa, \tag{5.11}$$

for all $\widehat{\Omega}_e \in \widehat{\mathcal{T}}_h$. It follows from Eqs. (2.2) and (2.3) that $\widehat{F} = \widehat{\breve{F}} \left\|\widehat{F}\right\|_{L^\infty(\widehat{\Omega}_e)}$, $\widehat{G} = \widehat{\breve{G}} \left\|\widehat{F}\right\|^2_{L^\infty(\widehat{\Omega}_e)}$, where $\widehat{\breve{G}} := \left(\widehat{\breve{F}}\right)^T \widehat{\breve{F}}$, from which we deduce that:

$$\widehat{F}\,\widehat{G}^{-1} = \widehat{\breve{F}}\,\widehat{\breve{G}}^{-1} \left\|\widehat{F}\right\|^{-1}_{L^\infty(\widehat{\Omega}_e)}. \tag{5.12}$$

In analogy with Eqs. (2.5) and (2.6), we define $\breve{F} \;:\; \breve{\Omega}_e \to \mathbb{R}^{d\times\kappa}$ with $\breve{F}(\mathbf{x}) := \widehat{\breve{F}}(\boldsymbol{\xi}) \circ \mathbf{x}^{-1}(\boldsymbol{\xi})$ and $\breve{G} \;:\; \breve{\Omega}_e \to \mathbb{R}^{\kappa\times\kappa}$ with $\breve{G}(\mathbf{x}) := \widehat{\breve{G}}(\boldsymbol{\xi}) \circ \mathbf{x}^{-1}(\boldsymbol{\xi})$, for all $\mathbf{x} \in \breve{\Omega}_e$; we obtain:

$$\left\|F\, G^{-1}\right\|_{L^\infty(\Omega_e)} \leq \left\|\breve{F}\,\breve{G}^{-1}\right\|_{L^\infty(\breve{\Omega}_e)} \left\|\widehat{F}\right\|^{-1}_{L^\infty(\widehat{\Omega}_e)}. \tag{5.13}$$

By setting $C_{shape} := \left\|\breve{F}\,\breve{G}^{-1}\right\|_{L^\infty(\breve{\Omega}_e)}$ and using the bound (5.13) in Eq. (5.9), we obtain the result (5.2).

The choice of the constant C_{shape} is justified similarly to [2] by observing that $\widehat{F}$ is 0–homogeneous with respect to $\breve{F}$ and that from Eq. (5.12) we have the following bound:

$$C_{shape} \leq \left\|F\, G^{-1}\right\|_{L^\infty(\Omega_e)} \left\|\widehat{F}\right\|_{L^\infty(\widehat{\Omega}_e)}; \tag{5.14}$$

hence, the constant C_{shape} only depends on the shape of the manifold and is uniformly bounded with respect to the "mesh" size h_e, since the NURBS mapping (2.1) is preserved under h–refinement. □

We recall from [2] the interpolation error estimate for the NURBS space on the parametric domain, which is obtained by using the concept of bent Sobolev space and combining the Eqs. (42) and (65) reported in [2]. With this aim, we introduce from Eq. (4.2) the projection operator $\Pi_{\widehat{\mathcal{N}}_h} : L^2(\widehat{\Omega}) \to \widehat{\mathcal{N}}_h$ onto the NURBS space in the parameter domain (see Eq. (41) in [2]).

Proposition 5.2. *Given the indexes k and l such that $0 \leq k \leq l \leq p+1$ and $k \leq 1$, the "mesh" element $\widehat{\Omega}_e \in \widehat{\mathcal{T}}_h$, its support extension $\widetilde{\widehat{\Omega}}_e$, and the function $\widehat{\phi} \in H^l(\widetilde{\widehat{\Omega}}_e)$, we have:*

$$\left|\widehat{\phi} - \Pi_{\widehat{\mathcal{N}}_h}\widehat{\phi}\right|_{H^k(\widehat{\Omega}_e)} \leq C_{shape}\, \widehat{h}_e^{l-k} \sum_{i=0}^{l} \sum_{\substack{\widehat{\Omega}'_e \in \widehat{\mathcal{T}}_h \\ \widehat{\Omega}'_e \cap \widetilde{\widehat{\Omega}}_e \neq \emptyset}} \left|\widehat{\phi}\right|_{H^i(\widehat{\Omega}'_e)}, \tag{5.15}$$

where $\widehat{h}_e$ is the characteristic size of the "mesh" element $\widehat{\Omega}_e$ in the parameter domain and C_{shape} is a positive and dimensionless constant depending on the NURBS parametrization but not on the size of $\widehat{\Omega}_e$.

Finally, we provide the interpolation error estimate for lower dimensional manifolds Ω defined by NURBS by introducing from Eq. (4.3) the projection operator $\Pi_{\mathcal{N}_h} : L^2(\Omega) \to \widehat{\mathcal{N}}_h$ onto the NURBS space in the physical domain, i.e. the "push–forward" of the NURBS projection operator, for which $\Pi_{\mathcal{N}_h}\phi(\mathbf{x}) = \left(\Pi_{\widehat{\mathcal{N}}_h}\widehat{\phi}(\boldsymbol{\xi})\right) \circ \mathbf{x}^{-1}(\boldsymbol{\xi})$ for all $\phi \in L^2(\Omega)$ ([2]).

Theorem 5.1. *Given the indexes k and l such that $0 \leq k \leq l \leq p+1$ and $k \leq 1$, the "mesh" element $\Omega_e \in \mathcal{T}_h$, its support extension $\widetilde{\Omega}_e$, and the function $\phi \in L^2(\Omega) \cap H^l(\widetilde{\Omega}_e)$, the interpolation error estimate for the NURBS space (4.3) on the lower dimensional manifold reads:*

$$|\phi - \Pi_{\mathcal{N}_h}\phi|_{H^k(\Omega_e)} \leq C_{shape}\, h_e^{l-k} \sum_{i=0}^{l} \left[\left\|\widehat{F}\right\|^{i-l}_{L^\infty(\widetilde{\widehat{\Omega}}_e)} |\phi|_{H^i(\widetilde{\Omega}_e)} \right], \tag{5.16}$$

where h_e is the characteristic size of the "mesh" element Ω_e (2.17), $\widetilde{\widehat{\Omega}}_e$ is the support extension of the "mesh" element in the parameter domain, and C_{shape} is a positive and dimensionless constant depending on the shape of the manifold Ω but not its size.

Proof. We start by observing that from the definition of the NURBS projector $\Pi_{\mathcal{N}_h}$ and Eq. (5.2), we have:

$$|\phi - \Pi_{\mathcal{N}_h}\phi|_{H^k(\Omega_e)} \leq C_{shape}\, \|\widehat{g}\|^{1/2}_{L^\infty(\widehat{\Omega}_e)} \left\|\widehat{F}\right\|^{-k}_{L^\infty(\widehat{\Omega}_e)} \sum_{i=0}^{k} \left|\widehat{\phi} - \Pi_{\widehat{\mathcal{N}}_h}\widehat{\phi}\right|_{H^i(\widehat{\Omega}_e)}. \tag{5.17}$$

By using the result (5.15) of Proposition 5.2 for the term $\left|\widehat{\phi} - \Pi_{\widehat{\mathcal{N}}_h}\widehat{\phi}\right|_{H^i(\widehat{\Omega}_e)}$, we obtain:

$$|\phi - \Pi_{\mathcal{N}_h}\phi|_{H^k(\Omega_e)} \leq C_{shape}\, \widehat{h}_e^{l-k}\, \|\widehat{g}\|^{1/2}_{L^\infty(\widehat{\Omega}_e)} \left\|\widehat{F}\right\|^{-k}_{L^\infty(\widehat{\Omega}_e)} \sum_{i=0}^{l} \sum_{\substack{\widehat{\Omega}'_e \in \widehat{\mathcal{T}}_h \\ \widehat{\Omega}'_e \cap \widetilde{\widehat{\Omega}}_e \neq \emptyset}} \left|\widehat{\phi}\right|_{H^i(\widehat{\Omega}'_e)}. \tag{5.18}$$

We apply the result (5.1) of Proposition 5.2 to each of the terms $\left|\widehat{\phi}\right|_{H^i(\widehat{\Omega}'_e)}$ which yields:

$$\left|\widehat{\phi}\right|_{H^i(\widehat{\Omega}'_e)} \leq C_{shape} \left\|\frac{1}{g}\right\|^{1/2}_{L^\infty(\Omega'_e)} \sum_{j=0}^{i} \left[\left\|\widehat{F}\right\|^{j}_{L^\infty(\widehat{\Omega}'_e)} |\phi|_{H^j(\Omega'_e)} \right], \tag{5.19}$$

for all $\widehat{\Omega}'_e \in \widehat{\mathcal{T}}_h$, where Ω'_e is obtained from the geometrical mapping of $\widehat{\Omega}'_e$. Then, by inserting Eq. (5.19) into Eq. (5.18), and merging the double summation over the indexes i and j, for which $0 \leq j \leq i$ and $0 \leq i \leq l$, we obtain:

$$|\phi - \Pi_{\mathcal{N}_h}\phi|_{H^k(\Omega_e)} \leq C_{shape}\, \widehat{h}_e^{l-k} \left\|\widehat{F}\right\|^{-k}_{L^\infty(\widehat{\Omega}_e)} \sum_{i=0}^{l} \left[\left\|\widehat{F}\right\|^{i}_{L^\infty(\widetilde{\widehat{\Omega}}_e)} |\phi|_{H^i(\widetilde{\Omega}_e)} \right], \tag{5.20}$$

where we used the bound:

$$\sum_{\substack{\widehat{\Omega}'_e \in \widehat{\mathcal{T}}_h \\ \widehat{\Omega}'_e \cap \widetilde{\widehat{\Omega}}_e \neq \emptyset}} \left[\left\|\frac{1}{g}\right\|^{1/2}_{L^\infty(\Omega'_e)} \left\|\widehat{F}\right\|^{i}_{L^\infty(\widehat{\Omega}'_e)} |\phi|_{H^i(\Omega'_e)} \right] \leq \left\|\frac{1}{g}\right\|^{1/2}_{L^\infty(\widetilde{\Omega}_e)} \left\|\widehat{F}\right\|^{i}_{L^\infty(\widetilde{\widehat{\Omega}}_e)} |\phi|_{H^i(\widetilde{\Omega}_e)}, \tag{5.21}$$

for all $i = 0, \ldots, l$, and the product $\|\widehat{g}\|^{1/2}_{L^\infty(\widehat{\Omega}_e)} \left\|\frac{1}{g}\right\|^{1/2}_{L^\infty(\widetilde{\Omega}_e)}$ has been embedded in the constant C_{shape}, similarly to the proof of Proposition 5.1 and Theorem 3.1 in [2]. We recall the definition of characteristic "mesh" size h_e of the element Ω_e on the manifold given in Eq. (2.17) to obtain from Eq. (5.20):

$$|\phi - \Pi_{\mathcal{N}_h}\phi|_{H^k(\Omega_e)} \leq C_{shape}\, h_e^{l-k} \left\|\widehat{F}\right\|^{-l}_{L^\infty(\widehat{\Omega}_e)} \sum_{i=0}^{l} \left[\left\|\widehat{F}\right\|^{i}_{L^\infty(\widetilde{\widehat{\Omega}}_e)} |\phi|_{H^i(\widetilde{\Omega}_e)} \right]. \tag{5.22}$$

Finally, by multiplying and dividing the right hand side of Eq. (5.22) by $\left\|\widehat{F}\right\|^{l}_{L^\infty(\widetilde{\widehat{\Omega}}_e)}$ and embedding the term $\left\|\widehat{F}\right\|^{l}_{L^\infty(\widetilde{\widehat{\Omega}}_e)} \left\|\widehat{F}\right\|^{-l}_{L^\infty(\widehat{\Omega}_e)}$ into the constant C_{shape} we obtain the result (5.16). □

In analogy with [2], a similar interpolation error estimation of Theorem 5.1 can be obtained for NURBS spaces with boundary conditions. Moreover, we remark that the interpolation error estimate (5.16) for lower dimensional manifolds assumes the same form of the result (61) of [2] in the case $\kappa = d$ (Theorem 3.1), where the differences between the two estimates have been embedded in the constant C_{shape}. When $\kappa = d$, the interpolation error estimate (5.16) fully coincides with the estimate of Theorem 3.1 in [2].

5.2 The Laplace–Beltrami equation

By using the result of Theorem 5.1, we provide the a priori error estimates in L^2 and H^1 norms for the Laplace–Beltrami problem of Sec. 3.2 defined on a general lower dimensional manifold Ω.

Following e.g. [15, 44], by recalling the notation for the NURBS spaces introduced in Sec. 4.1 and assuming the Laplace–Beltrami problem (3.10) to be well–posed, we have:

$$|u - u_h|_{H^1(\Omega)} \leq C \inf_{v_h \in \mathcal{V}_{\gamma,h}} |u - v_h|_{H^1(\Omega)}, \tag{5.23}$$

where the positive constant C depends on the data of the problem, specifically the coefficient μ ($C = C(\mu)$). From the result (5.16) of Theorem 5.1, by assuming quasi uniform h–refinement, the

"mesh" elements of size $h_e \simeq h$ for all $e = 1, \dots, n_{el}$, and the polynomial orders of the NURBS basis $\min_{\alpha=1,\dots,\kappa} p_\alpha = p$, we obtain the error estimate in semi–norm H^1 for the case $u \in H^{p+1}(\Omega)$:

$$|u - u_h|_{H^1(\Omega)} \leq C\, h^p, \tag{5.24}$$

where the positive constant C depends on μ, u, and the constant C_{shape}. Further, if we assume that homogeneous Dirichlet boundary conditions ($\gamma = 0$) and $u \in H^{p+1}(\Omega) \cap H^2(\Omega)$ for all the data, we obtain from standard Aubin–Niestche arguments the error estimate in norm L^2 (see e.g. [49]):

$$err_{L^2} := \|u - u_h\|_{L^2(\Omega)} \leq C\, h^{p+1}, \tag{5.25}$$

from which we deduce the error estimate in norm H^1:

$$err_{H^1} := \|u - u_h\|_{H^1(\Omega)} = \left(err_{L^2}^2 + |u - u_h|_{H^1(\Omega)}^2\right)^{1/2} \leq C\, h^p. \tag{5.26}$$

Similar considerations follow in the case for which the Laplace–Beltrami problem (3.10) is defined on lower dimensional manifolds Ω not endowed with boundary; in this case, the analysis is performed by considering the function space $\mathcal{V}_0$ in place of $\mathcal{V}_\gamma$ according to Sec. 3.2, which yields a similar result.

5.3 The Laplace–Beltrami eigenvalue problem

We provide the a priori error estimate for the numerical approximation of the Laplace–Beltrami eigenvalue problem of Sec. 3.3 on the lower dimensional manifold Ω. We consider the error on the eigenvalues of the problem, say $|\lambda_n - \lambda_{n,h}|$, where n indicates the n–the eigenvalue and $\lambda_{n,h}$ corresponds to its numerical approximation for $n = 0, 1, \dots$ (see e.g. Eq. (4.5)); specifically, we consider the ordering $\lambda_0 \leq \lambda_1 \leq \dots \leq \lambda_n \leq \dots$ by recalling that the eigenvalues of the Laplace–Beltrami eigenvalue problem (3.12) are real and non negative.

From [49] we have that, for the Laplace–Beltrami eigenvalue problem under consideration:

$$\lambda_{n,h} \leq \frac{\lambda_n}{1 - \varrho_{n,h}} \qquad \forall n \geq 0, \tag{5.27}$$

where from Eq. (3.3):

$$\varrho_{n,h} := \max_{\substack{v \in \mathcal{V}_n \\ \|v\|_{L^2(\Omega)} = 1}} \left| 2\, m\left(v - \Pi_{\mathcal{V}_h}^E v, v\right) - m\left(v - \Pi_{\mathcal{V}_h}^E v, v - \Pi_{\mathcal{V}_h}^E v\right) \right| \qquad \forall n \geq 0, \tag{5.28}$$

with $\mathcal{V}_n \subseteq \mathcal{V}$ the n–dimensional subspace spanned by the eigenfunctions $u_1, \dots, u_n$ and being $\Pi_{\mathcal{V}_h}^E : \mathcal{V} \to \mathcal{V}_h$ the Rayleigh–Ritz projector into the NURBS space on the physical domain (manifold) which yields, for some $\phi \in \mathcal{V}$, $a(v_h, \phi - \Pi_{\mathcal{V}_h}^E \phi) = 0$ for all $v_h \in \mathcal{V}_h$. Since the NURBS space $\mathcal{N}_h$ is conforming with the function space $\mathcal{V}$, by using the standard arguments presented in [49] (or [7]) and the interpolation error estimate (5.16) of Theorem 5.1, we obtain:

$$\lambda_n \leq \lambda_{n,h} \leq \lambda_n + C\, (\lambda_n)^{p+1}\, h^{2p} \qquad \forall n \geq 0, \tag{5.29}$$

provided that the "mesh" size h is sufficiently small (with $h_e \simeq h$ for all the elements $\Omega_e \in \mathcal{T}_h$) and the polynomial orders of the NURBS basis such that $\min_{\alpha=1,\dots,\kappa} p_\alpha = p$; the positive constant C

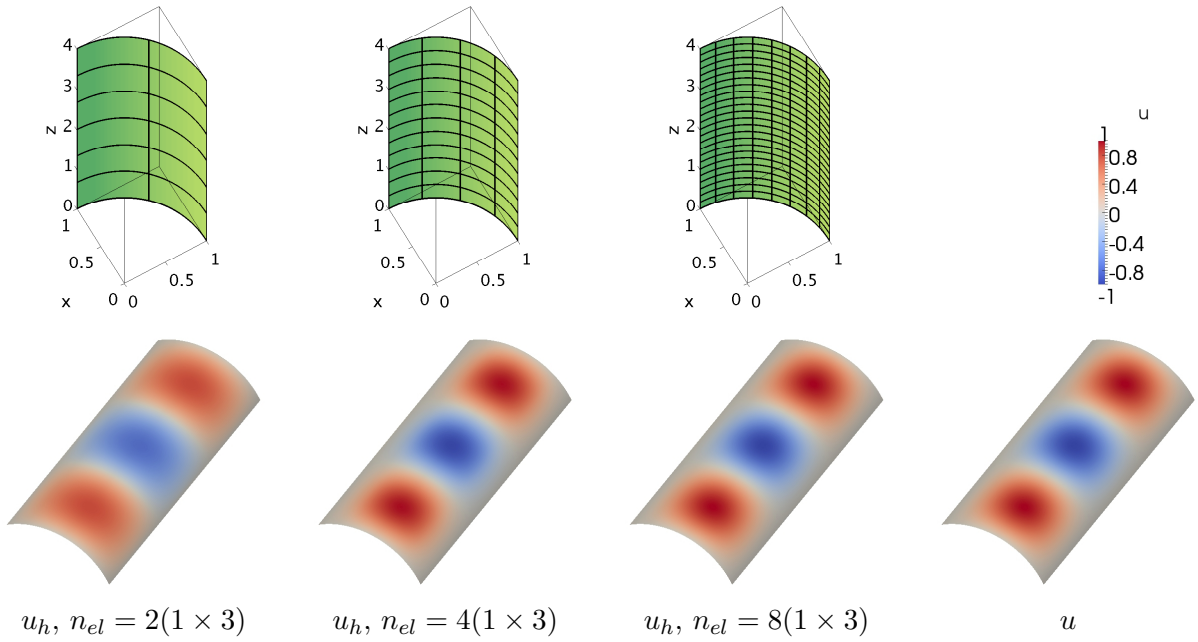

Figure 4: Laplace–Beltrami problem on a cylindrical shell. h–refined "meshes" (top), corresponding numerical solutions u_h (bottom), and exact solution u (bottom–right).

depends on the data of the Laplace–Beltrami operator and the constant C_{shape}. It follows that the error associated to the n–th eigenvalue, say err_n, can be estimated as:

$$err_n := \lambda_{n,h} - \lambda_n \sim C\ (\lambda_n)^{p+1}\ h^{2p} \qquad \forall n \geq 0, \tag{5.30}$$

which highlights the convergence rate $2p$ for h–refined mesh in agreement with the error estimates for the Finite Element method in the case $\kappa = d$; see e.g. [44, 49]. We remark that, when λ_n is "large" the error err_n could be significantly "large" also for fine "meshes" being the error proportional to $(\lambda_n)^{p+1}$.

6 Numerical results: PDEs on surfaces

We consider the numerical solution of the problems defined in Sec. 3 for the specific cases of surfaces as lower dimensional manifolds.

6.1 The Laplace–Beltrami equation

We numerically solve the Laplace–Beltrami equation (3.10) on two surfaces, we evaluate the errors between the numerical and exact solutions and we estimate the convergence orders of such errors for the polynomial orders $p = 2$ and 3 of the NURBS basis.

Firstly, we consider as computational domain Ω a quarter of the cylinder represented in Fig. 3 (left) (corresponding to the quadrant with x ≥ 0 and y ≥ 0) with unitary radius and height L. We choose $\mu = 1$ and $f(\phi, z) = \beta \left(\dfrac{\alpha^2 \pi^2}{L^2} g_{\phi,1}(\phi) - g_{\phi,2}(\phi) \right) g_{\mathrm{z}}(\mathrm{z})$, where $\phi := \mathrm{atan}\left(\dfrac{\mathrm{x}}{\mathrm{y}}\right)$, $g_{\phi,1}(\phi) :=$

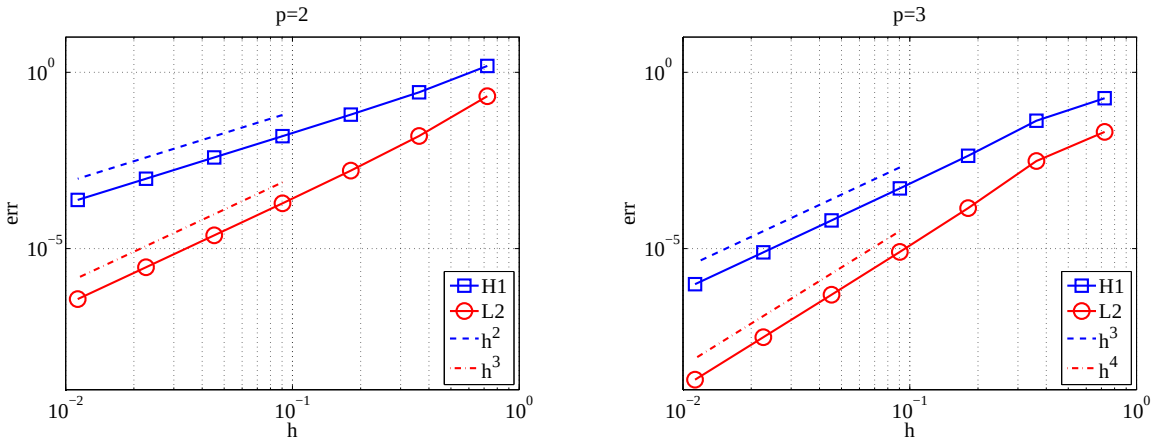

Figure 5: Laplace–Beltrami problem on a cylindrical shell. Convergence of the errors err_{H^1} (—□) and err_{L^2} (—○) and reference convergences rates p (- -) and $p+1$ (. -) vs. the "mesh" size h for $p=2$ (left) and $p=3$ (right).

$(1-\cos(\phi))\,(1-\sin(\phi))$, $g_{\phi,2}(\phi) := (\cos(\phi)+\sin(\phi)-4\,\sin(\phi)\,\cos(\phi))$, and $g_{\mathrm{z}}(\mathrm{z}) := \sin\left(\alpha\,\pi\,\dfrac{\mathrm{z}}{L}\right)$ for $\alpha \in \mathbb{N}_0$ and $\beta > 0$; then, we set $u(\mathbf{x}) = \gamma(\mathbf{x}) = 0$ on Γ. The exact solution of the problem reads $u(\phi,\mathrm{z}) = \beta\, g_{\phi,1}(\phi)\, g_{\mathrm{z}}(\mathrm{z})$ in cylindrical coordinates. Specifically, we select $\alpha = 3$, $\beta = 1/\left(3/2-\sqrt{2}\right)$, and $L = 4$. We solve the problem by meas of Isogeometric Analysis with NURBS basis functions of order $p = 2$ and $p = 3$ for different "mesh" sizes starting from a mesh with 2 elements in the circumferential direction. The exact and numerical solution and corresponding "meshes" are reported in Fig. 4; we highlight the smoothness of the approximated solutions in circumferential direction even for a small number of "mesh" elements. The convergence rates of the errors are reported in Fig. 5 for the polynomial orders $p = 2$ and 3; in particular, we obtain the convergence rates $p+1$ and p for the norms L^2 and H^1, respectively. The convergence rates are in agreement with the expected theoretical ones reported in Sec. 5.2 since the exact solution is "sufficiently" regular, i.e. $u \in C^\infty(\Omega) \cap H^{p+1}(\Omega)$.

Then, we consider a Laplace–Beltrami problem with exact solution on the sphere of unitary radius reported in Fig. 3 (right); since the surface is closed ($\Gamma \equiv \emptyset$), we impose the constraint $\displaystyle\int_\Omega u\, d\Omega = 0$. We set $f(\phi,\theta) = \sin(\alpha\phi)\sin(\beta\theta)\left[\dfrac{\alpha^2}{\sin^2(\theta)} + \beta^2 - \beta\,\dfrac{\cos(\theta)\,\cos(\beta\theta)}{\sin(\theta)\,\sin(\beta\theta)}\right]$ with $\phi := \mathrm{atan2}\left(\dfrac{\mathrm{x}}{\mathrm{y}}\right)$, $\theta := \mathrm{acos}\left(\dfrac{\mathrm{z}}{\mathrm{r}}\right)$, $\alpha > 0$, $\beta > 0$, and $\mu = 1$. The exact solution in spherical coordinates reads $u(\phi,\theta) = \sin(\alpha\phi)\,\sin(\beta\theta)$. In particular, we choose $\alpha = 3$ and $\beta = 4$. We report in Fig. 6 the exact and numerical solutions corresponding to "meshes" progressively h–refined; we remark the smoothness of the numerical solution along both the parametric directions even for the coarsest "meshes". In Fig. 7 we highlight the convergence rates of the errors err_{L^2} and err_{H^1} which are in agreement with the theoretical ones, being the exact solution $u \in C^\infty(\Omega) \cap H^{p+1}(\Omega)$ as highlighted in Sec. 5.2.

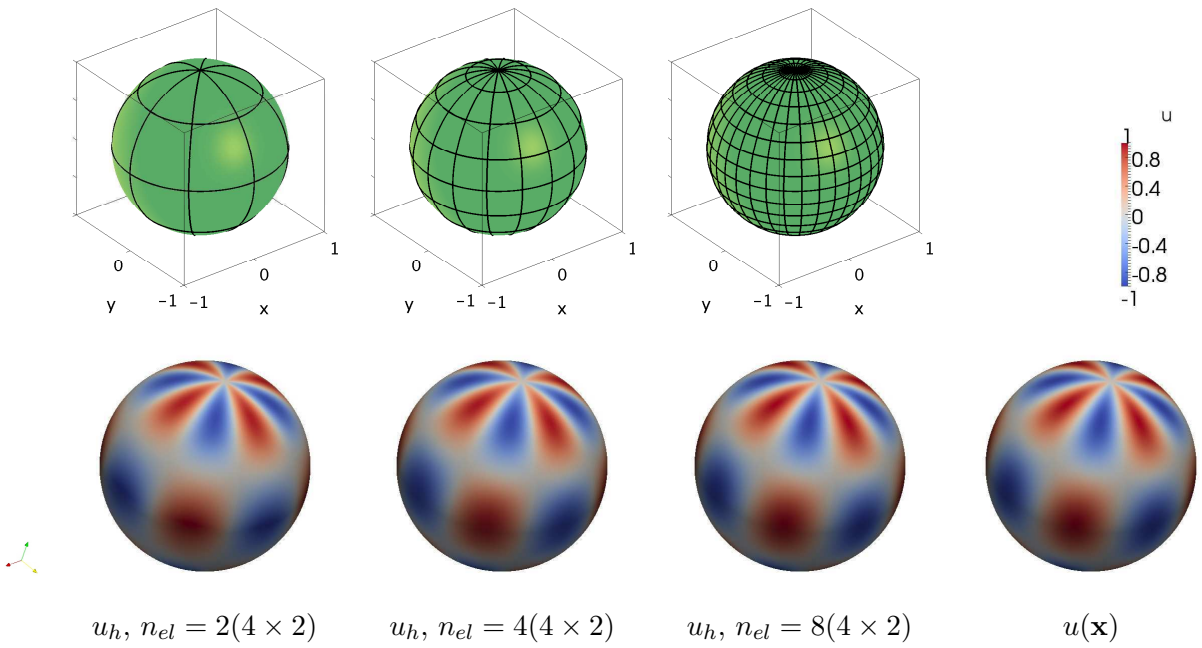

Figure 6: Laplace–Beltrami problem on a sphere. h–refined "meshes" (top), corresponding numerical solutions u_h (bottom), and exact solution u (bottom–right).

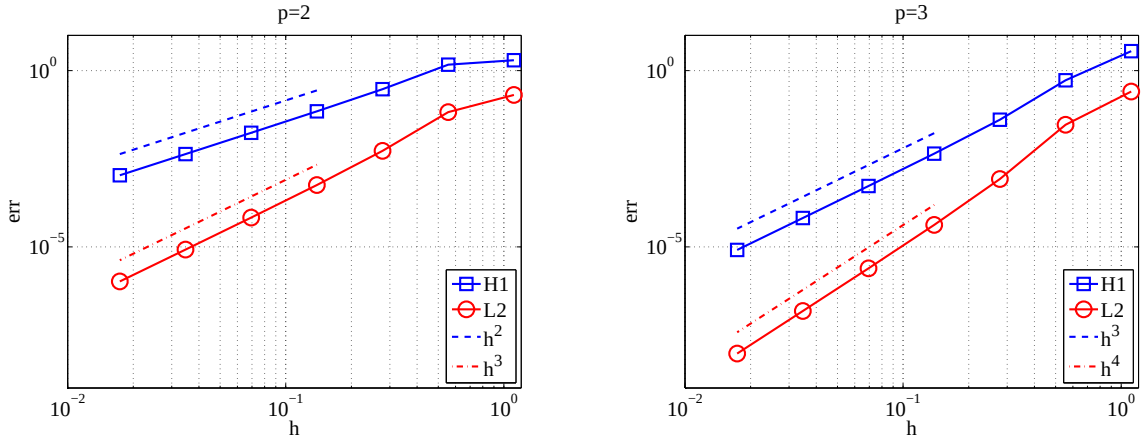

Figure 7: Laplace–Beltrami problem on a sphere. Convergence of the errors err_{H^1} (—□) and err_{L^2} (—○) and reference convergences rates p (- -) and $p+1$ (. -) vs. the "mesh" size h for $p = 2$ (left) and $p = 3$ (right).

6.2 The Laplace–Beltrami eigenvalue problem

We consider the numerical approximation of the eigenvalue problem (3.12) associated to the Laplace–Beltrami operator on the sphere of unitary radius of Fig. 3 (right). The exact values of the eigenvalues are $\lambda_n = n(n+1)$, each with multiplicity $2n+1$, for $n = 0, 1, \ldots, \infty$ (see e.g.

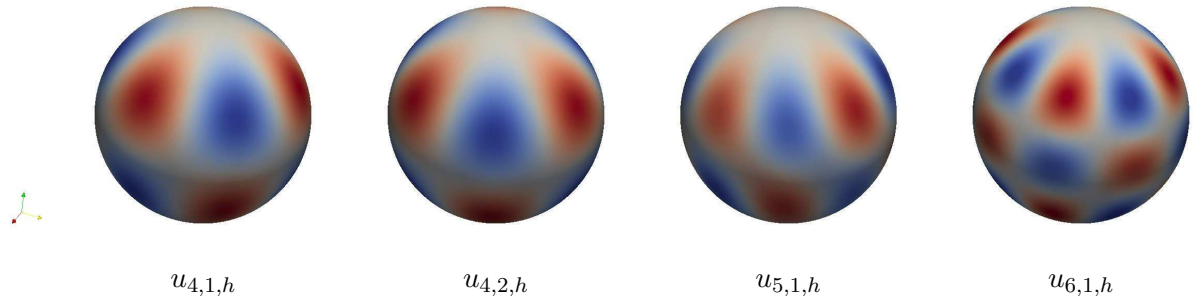

Figure 8: Eigenvalue problem on a sphere. Eigenfunctions $u_{4,1,h}$, $u_{4,2,h}$, $u_{5,1,h}$, and $u_{6,1,h}$ (from left to right).

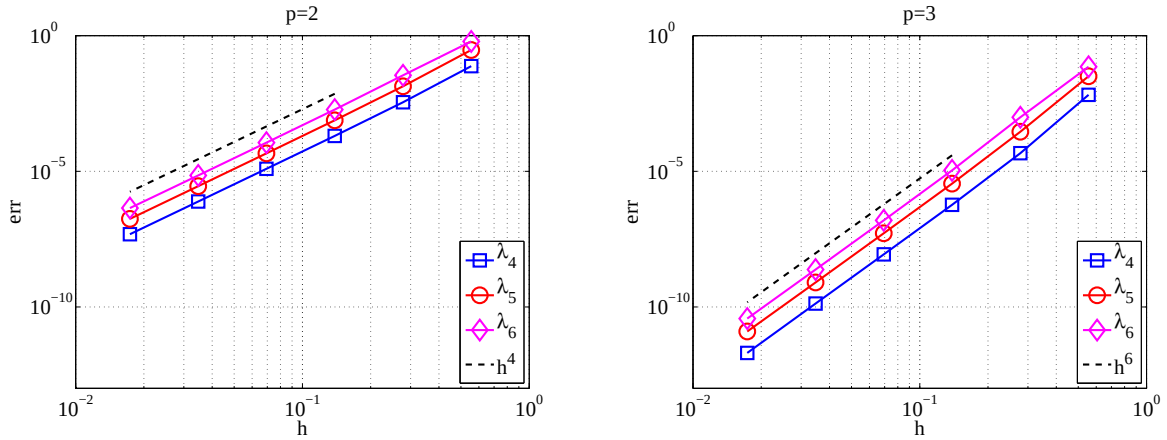

Figure 9: Eigenvalue problem on a sphere. Convergence of the errors err_n on the eigenvalues λ_n vs. the "mesh" size h for $n = 4$ (—□), $n = 5$ (—○), and $n = 6$ (—◇) and reference convergences rate $2p$ (- -) for $p = 2$ (left) and $p = 3$ (right).

[45]), to which correspond the eigenfunctions u_{n,l_n}, with $l_n = 1, \dots, 2n+1$. We numerically approximate the problem by means of Isogeometric Analysis on a "mesh" with $n_{el} = 131,072$ elements and basis functions of order $p = 2$; in Fig. 8 we report for example the computed eigenfunctions $u_{4,1,h}$, $u_{4,2,h}$, $u_{5,1,h}$, and $u_{6,1,h}$ corresponding to the eigenvalues $\lambda_4 = 20$, $\lambda_5 = 30$, and $\lambda_6 = 42$, respectively. In Fig. 9 we report the errors on the eigenvalues λ_4, λ_5, and λ_6 ($err_n = |\lambda_n - \lambda_{n,h}|$), vs. the "mesh" size h when considering basis functions of order $p = 2$ and $p = 3$. As expected by the theoretical result (5.30) of Sec. 5.3, the convergence rate obtained for the numerical results correspond to $2p$.

6.3 The time dependent linear advection–diffusion equation

We consider the time dependent linear advection–diffusion equation on the cylindrical shell reported in Fig. 3 (left). By using the notation of Sec. 3.4 and using cylindrical coordinates, we set $\mathbf{V}(\phi, \mathrm{z}) = \dfrac{V_0}{\sqrt{1+a^2}}(\widehat{\boldsymbol{\phi}} + a\widehat{\mathbf{z}})$, and $f(\phi, \mathrm{z}) = e^{-b\left((\phi-\phi_0)^2+(z-z_0)^2\right)}$, where $\phi := \mathrm{atan2}\left(\dfrac{\mathrm{x}}{\mathrm{y}}\right)$, V_0, a, ϕ_0, and $z_0 \in \mathbb{R}$;

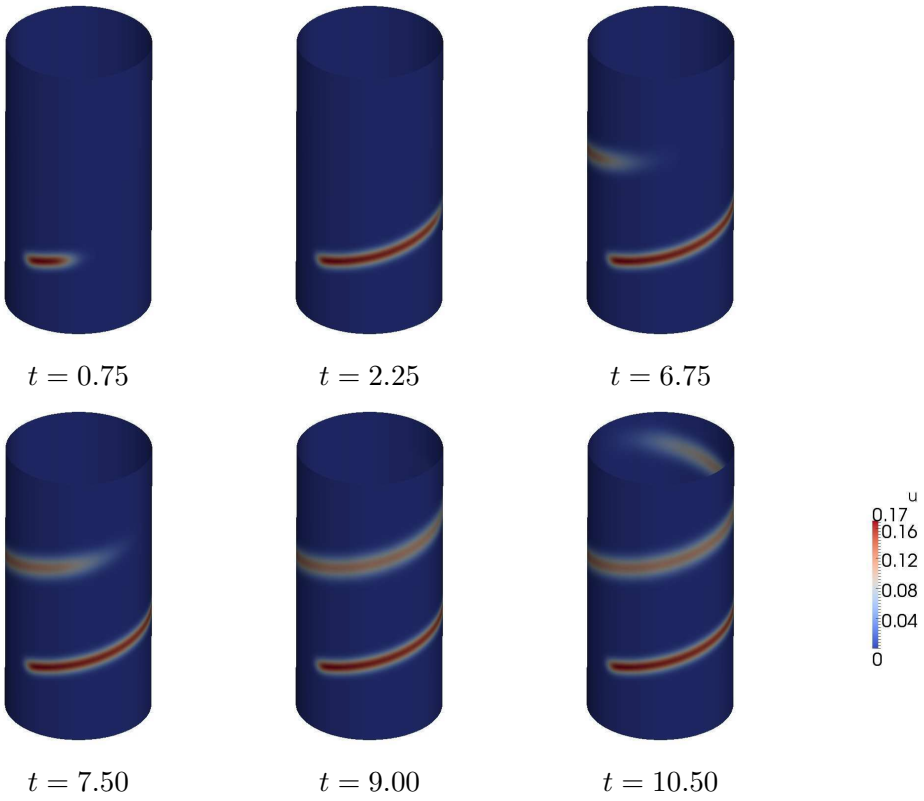

Figure 10: Time dependent advection–diffusion problem on a cylindrical shell. Evolution of the solution in time.

we set homogeneous Neumann conditions on the boundary $\Gamma = \Gamma_N$ and $u_{in}(\mathbf{x}) = 0$. In particular, we set $\mu = 5.0 \cdot 10^{-4}$, $V_0 = 1$, $a = 0.2$, $b = 100$, $\phi_0 = \dfrac{\pi}{4}$, and $z_0 = 0.5$. We numerically solve the problem by means of Isogeometric Analysis with the SUPG stabilization technique discussed in Sec. 4.3. A NURBS representation with basis of order $p = 2$ and comprised of $n_{el} = 12,288$ "mesh" elements is considered. For the time discretization, the generalized–α method of Sec. 4.2 is used with the fixed time step $\Delta t_0 = 1.5 \cdot 10^{-2}$. In Fig. 10 we report the evolution of the solution in time; we highlight its helical distribution along the surface of the cylindrical shell induced by the advective field.

6.4 The Cahn–Allen problem

We solve the Cahn–Allen problem defined in Sec. 3.5 on the sphere of unitary radius of Fig. 3 (right). By using the notation of Sec. 3.5, we select $\mu = 5.0 \cdot 10^{-4}$ and $u_{in} = u_0 + \varepsilon$, where $u_0 = 0.5$ and ε is a random distribution such that $|\varepsilon| \leq 0.1$. We numerically solve the problem by means of Isogeometric Analysis with NURBS basis functions of order $p = 2$ and a "mesh" comprised of $n_{el} = 32,768$ elements; the time approximation is based on the generalized–α method with the adaptive time stepping scheme initialized with the time step $\Delta t_0 = 5.0 \cdot 10^{-1}$. In Fig. 11 we report the evolution of the concentration $u(\mathbf{x}, t)$ in time. The phase transition evolves towards the steady state to a configuration with the phases fully separated with a minimum perimeter interface.

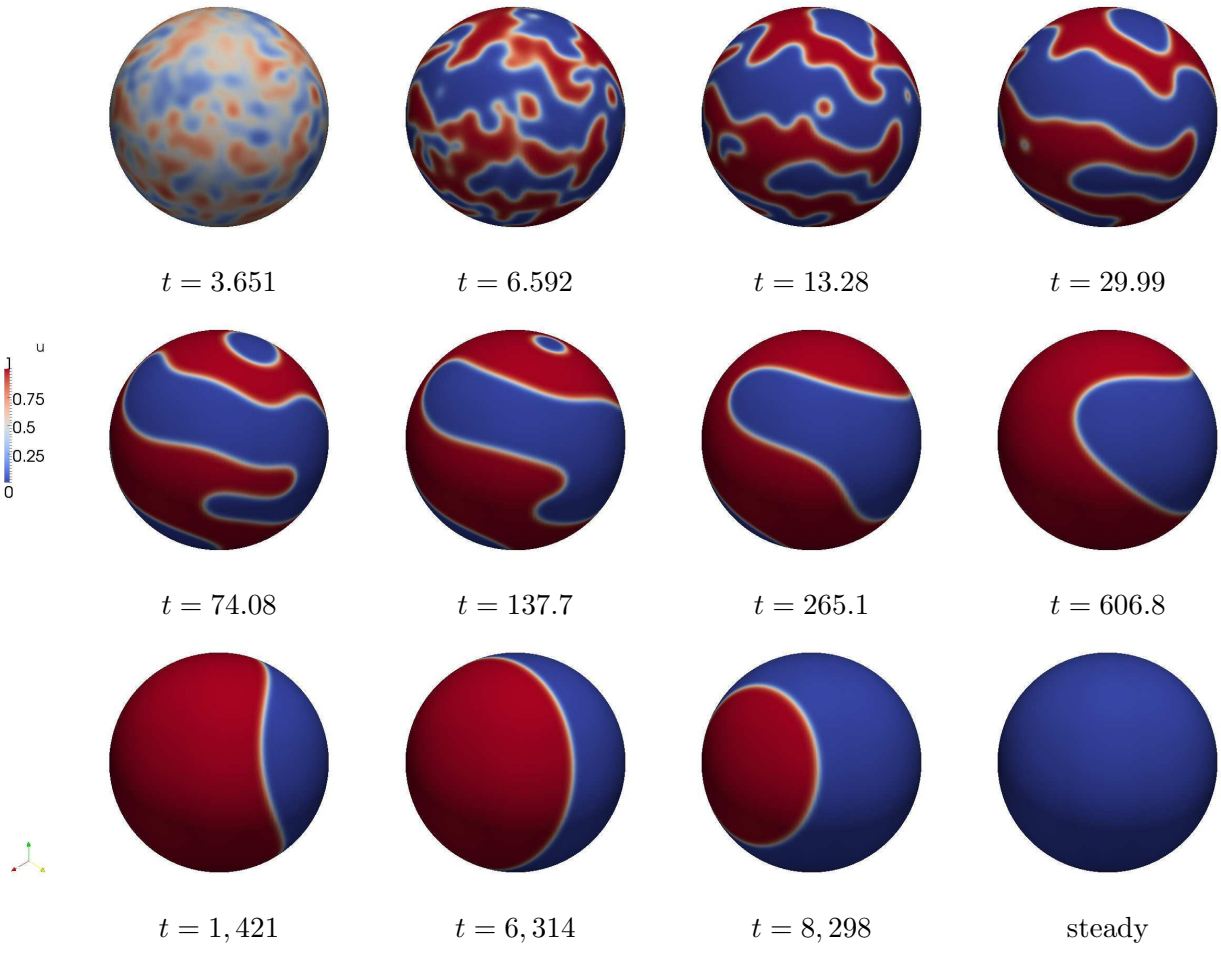

Figure 11: Cahn–Allen equation on a sphere. Evolution of the solution in time.

However, due to the fact that the Cahn–Allen equation does not represent a mass conservative system, the solution evolves to a pure phase at the steady state, which corresponds to $u = 0$ in the case under consideration, since $\int_\Omega u_{in}\, d\Omega < u_0 = 0.5$. In Fig. 12 we report the evolution of the (Liapunov) free energy functional $\widetilde{\Psi}(t)$ for which we observe that $\dfrac{d\widetilde{\Psi}}{dt}(t) \leq 0$.

7 Conclusions

In this work we showed the efficacy of Isogeometric Analysis for the numerical approximation of PDEs defined on lower dimensional manifolds, specifically on surfaces. We considered different linear and nonlinear, elliptic and parabolic PDEs with second order spatial operators of the Laplace–Beltrami type; examples include the eigenvalue problem, the time dependent advection–diffusion equation, and the Cahn–Allen equation. We highlighted the capability of Isogeometric Analysis of facilitating the encapsulation of the exact surface representations in the analysis at their coarsest

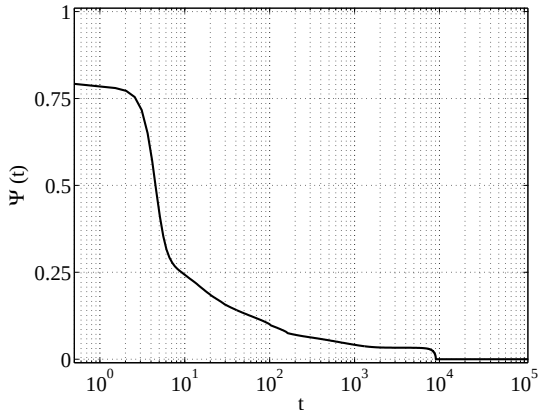

Figure 12: Cahn–Allen equation on a sphere. Evolution of the free energy $\widetilde{\Psi}(t)$ in time.

level of discretization, especially for geometries as cylindrical and spherical shells represented by NURBS. Moreover, we provided a priori error estimates under h–refinement for the numerical approximation of second order PDEs on general lower dimensional manifolds in the case of linear and eigenvalues problems associated to the Laplace–Beltrami operator. Specifically, the convergence rates of the errors are numerically confirmed for benchmark tests cases which highlight the effect of the accurate geometrical description on the computation of the numerical solutions.

Acknowledgements

We acknowledge Dmitry Alexeev for providing some preliminary insights into the topic and Claudia Colciago and Anna Tagliabue for the fruitful discussions.

References

[1] M. Berger. *A Panoramic View of Riemannian Geometry*. Springer–Verlag, Berlin and Heidelberg, 2003.

[2] Y. Bazilevs, L. Beirão da Veiga, J.A. Cottrell, T.J.R. Hughes, and G. Sangalli. Isogeometric Analysis: approximation, stability, and error estimates for h–refined meshes. *Mathematical Models and Methods for Applied Sciences* **16**(7):1031–1090, 2006.

[3] Y. Bazilevs, V.M. Calo, J.A. Cottrell, T.J.R. Hughes, A. Reali, and G. Scovazzi. Variational multiscale residual–based turbulence modeling for large eddy simulation of incompressible flows. *Computer Methods in Applied Mechanics and Engineering* **197**(1–4):173–201, 2007.

[4] L. Beirão da Veiga, A. Buffa, J. Rivas, and G. Sangalli. Some estimates for $h-p-k$–refinement in Isogeometric Analysis. *Numerische Mathematik* **118**(2):271–305, 2011.

[5] M. Beltramío, L.–T. Cheng, S. Osher, and G. Sapiro. Variational problems and partial differential equations on implicit surfaces. *Journal of Computational Physics* **174**(2): 759-780, 2001.

[6] D.J. Benson, Y. Bazilevs, M.C. Hsu, and T.J.R. Hughes. Isogeometric shell analysis: the Reissner-Mindlin shell. *Computer Methods in Applied Mechanics and Engineering* **199**(5–8):276–289, 2010.

[7] D. Boffi. Finite element approximation of eigenvalue problems. *Acta Numerica* **19**:1–120, 2010.

[8] A. Bonito, R.H. Nochetto, and S.M. Pauletti. Dynamics of biomembranes: effect of the bulk fluid. *Mathematical Modelling of Natural Phenomena* **6**(5):25–43, 2011.

[9] A. Bonito, R.H. Nochetto, and S.M. Pauletti. Geometrically consistent mesh modification. *SIAM Journal on Numerical Analysis* **48**(5):1877–1899, 2010.

[10] A.N. Brooks and T.J.R. Hughes. Streamline upwind/Petrov–Galerkin formulations for convection dominated flows with particular emphasis on the incompressible Navier–Stokes equations. *Computer Methods in Applied Mechanics and Engineering* **32**(1–3):199–259, 1982.

[11] J.W. Cahn. On spinodal decomposition. *Acta Metallurgica* **9**(9):795-801, 1961.

[12] J.W. Cahn and J.E. Hilliard. Free energy of a non–uniform system. I. Interfacial free energy. *Journal of Chemical Physics* **28**(2):258–267, 1958.

[13] W.C. Carter, J. Taylor, and J.W. Cahn. Variational methods for microstructural-evolution theories. *JOM Journal of the Minerals, Metals and Materials Society* **49**(12):30-36, 1997.

[14] J. Chung and G.M. Hulbert. A time integration algorithm for structural dynamics with improved numerical dissipation: the generalized α–method. *Journal of Applied Mechanics* **60**(2):371–375, 1993.

[15] P.G. Ciarlet. *The Finite Element Method for Elliptic Problems*. North–Holland, 1978.

[16] P.G. Ciarlet and P.–A. Raviart. Interpolation theory over curved elements, with applications to finite element methods. *Computer Methods in Applied Mechanics and Engineering* **1**(2):217–249, 1972.

[17] S. Coriasco, E. Schrohe, and J. Seiler. Differential operators on conic manifolds: maximal regularity and parabolic equations. *Bullettin de la Société Royale de Sciences de Liège* **70**(4–6):207–229, 2001.

[18] J.A. Cottrell, T.J.R. Hughes, and Y. Bazilevs. *Isogeometric Analysis: toward integration of CAD and FEA*. Wiley, 2009.

[19] J.A. Cottrell, T.J.R. Hughes, and A. Reali. Studies of refinement and continuity in isogeometric structural analysis. *Computer Methods in Applied Mechanics and Engineering* **196**(41–44):4160–4183, 2007.

[20] L. Dedè, M.J. Borden, and T.J.R. Hughes. Topology optimization with Isogeometric Analysis in a phase field approach. *Archives in Computational Methods in Engineering* **19**(3):427–465, 2012.

[21] M.C. Delfour and J.–P. Zolésio. *Shapes and Geometries: Analysis, Differential Calculus, and Optimization*. Advances in Design and Control 4, SIAM, Philadelphia, PA, 2001.

[22] G. Dziuk. Finite elements for the Beltrami operator on arbitrary surfaces. In *Partial differential equations and calculus of variations*, 142–155, Lecture Notes in Mathematics **1357**, 1988.

[23] G. Dziuk and C.M. Elliott. Eulerian finite element method for parabolic PDEs on implicit surfaces. *Interfaces and Free Boundaries* **10**:119-138, 2008.

[24] G. Dziuk and C.M. Elliott. Surface finite elements for parabolic equations. *Journal of Computational Mathematics* **25**(4):385–407, 2007.

[25] C.M. Elliott and H. Garcke. Existence results for diffusive surface motion laws. *Advances and Applications in Mathematical Sciences* **7**(1):465–488, 1997.

[26] C.M. Elliott and H. Garcke. On the Cahn–Hilliard equation with degenerate mobility. *SIAM Journal on Mathematical Analysis* **27**(2):404–423, 1996.

[27] J. Escher, U.F. Mayer, and G. Simonett. The surface diffusion flow for immersed hypersurfaces. *SIAM Journal on Mathematical Analysis* **29**(6):1419–1433, 1998.

[28] J.A. Evans, Y. Bazilevs, I. Babuška, and T.J.R. Hughes. n–widths, sup–infs, and optimality ratios for the k–version of the Isogeometric finite element method. *Computer Methods in Applied Mechanics and Engineering* **198**(21–26):1726–1741, 2009.

[29] P.C. Fife. Models for phase separation and their mathematics. *Electronic Journal of Differential Equations* **48**:1-26, 2000.

[30] L.P. Franca, S.L. Frey, T.J.R. Hughes. Stabilized finite element methods: I. Application to the advective–diffusive model. *Computer Methods for Applied Mechanics in Engineering* **95**(2):253–276, 1992.

[31] H. Gomez, V.M. Calo, Y. Bazilevs, and T.J.R. Hughes. Isogeometric analysis of the Cahn-Hilliard phase-field model. *Computer Methods for Applied Mechanics in Engineering* **197**(49–50):4333–4352, 2008.

[32] J.B. Greer, A.L. Bertozzi, and G. Sapiro. Fourth order partial differential equations on general geometries. *Journal of Computational Physics* **216**(1):216–246, 2006.

[33] T.J.R. Hughes. *The Finite Element Method: Linear Static and Dynamic Finite Element Analysis*. Dover Publications, Mineola, 2000.

[34] T.J.R. Hughes, J.A. Cottrell, and Y. Bazilevs. Isogeometric analysis: CAD, finite elements, NURBS, exact geometry and mesh refinement. *Computer Methods in Applied Mechanics and Engineering* **194**(39–41):4135–4195, 2005.

[35] T.J.R. Hughes, G. Scovazzi, and L.P. Franca. Multiscale and stabilized methods. In *Encyclopedia of Computational Mechanics*, E. Stein, R. de Borst, and T.J.R. Hughes (eds.). John Wiley & Sons, 2004.

[36] K.E. Jansen, C.H. Whiting, and G.M. Hulbert. A generalized–α method for integrating the filtered Navier-Stokes equations with a stabilized finite element method. *Computer Methods in Applied Mechanics and Engineering* **190**(3–4):305–319, 2000.

[37] J. Liu, L. Dedè, J.A. Evans, M.J. Borden, and T.J.R. Hughes. Isogeometric Analysis of the advective Cahn–Hilliard equation: spinodal decomposition under shear flow. *ICES report, The University of Texas at Austin* **12–12**, 2012. `http://www.ices.utexas.edu`

[38] K. Mekchay, P. Morin, and R.H. Nochetto. AFEM for the Laplace–Beltrami operator on graphs: design and conditional contraction property. *Mathematics of Computations* **80**(274):625–648, 2011.

[39] M.A. Olshanskii, A. Reuskeny, and X. Xu. A stabilized Finite Element method for advection–diffusion equations on surfaces. *Institut für Geometrie und Praktische Mathematik, RWTH Aachen, Preprint* **344**, 2012. `http://www.igpm.rwth-aachen.de`

[40] L. Piegl and W. Tiller. *The NURBS Book*. Springer–Verlag, New York, 1997.

[41] A. Quarteroni, R. Sacco, and F. Saleri. *Numerical Mathematics*. Springer, Berlin and Heidelberg, 2007.

[42] A. Quarteroni and A. Valli. *Numerical Approximation of Partial Differential Equations*. Springer–Verlag, Berlin, Heidelberg, 1994.

[43] A. Rätz and A. Voigt. PDE's on surfaces – a diffuse interface approach. *Communications in Mathematical Sciences* **4**(3):575–590, 2006.

[44] P.–A. Raviart and J.–M. Thomas. *Introduction à l'Analyse Numérique des Équations aux Dérivées Partielles*. Masson, Paris, 1983.

[45] M. Reuter, F.–E. Wolter, M. Shenton, and M. Niethammer. Laplace–Beltrami eigenvalues and topological features of eigenfunctions for statistical shape analysis. *Journal Computer–Aided Design* **41**(10):739–755, 2009.

[46] M.A. Scott, R.N. Simpson, J.A. Evans, S. Lipton, S.P.A. Bordas, T.J.R. Hughes, and T.W. Sederberg. Isogeometric boundary element analysis using unstructured T–splines. *ICES report, The University of Texas at Austin* **12–23**, 2012. `http://www.ices.utexas.edu`

[47] T.W. Sederberg, J.M. Zhengs, and J.M. Bakenov. T–splines and T–NURCCSs. *ACM Transactions on Graphics* **22**(3):477–484, 2003.

[48] F. Shakib, T.J.R. Hughes, and Z. Johan. A new finite element formulation for computational fluid dynamics: X. The compressible Euler and Navier–Stokes equations. *Computer Methods in Applied Mechanics and Engineering* **89**(1–3):141–219, 1991.

[49] G. Strang and G.J. Fix. *An Analysis of the Finite Element Method*. Prentice–Hall, Inc., Englewood Cliffs, N.J., 1973.

[50] S.P. Timoshenko and S. Woinowsky–Krieger. *Theory of Plates and Shells*. McGraw–Hill, New York, 1959.

[51] O. Wodo and B. Ganapathysubramanian. Computationally efficient solution to the Cahn-Hilliard equation: adaptive implicit time schemes, mesh sensitivity analysis and the 3D isoperimetric problem. *Journal of Computational Physics* **230**(15):6037–6080, 2011.

[52] L.C. Wrobel and M.H. Aliabadi. *The Boundary Element Method*. Wiley, Chichester, 2002.

MOX Technical Reports, last issues

Dipartimento di Matematica "F. Brioschi",
Politecnico di Milano, Via Bonardi 9 - 20133 Milano (Italy)

06/2013 Ded, L.; Quarteroni, A.
Isogeometric Analysis for second order Partial Differential Equations on surfaces

05/2013 Caputo, M.; Chiastra, C.; Cianciolo, C.; Cutri , E.; Dubini, G.; Gunn, J.; Keller, B.; Zunino, P.;
Simulation of oxygen transfer in stented arteries and correlation with in-stent restenosis

04/2013 Morlacchi, S.; Chiastra, C.; Cutr, E.; Zunino, P.; Burzotta, F.; Formaggia, L.; Dubini, G.; Migliavacca, F.
Stent deformation, physical stress, and drug elution obtained with provisional stenting, conventional culotte and Tryton-based culotte to treat bifurcations: a virtual simulation study

03/2013 Antonietti, P.F.; Ayuso de Dios, B.; Bertoluzza, S.; Pennacchio, M.
Substructuring preconditioners for an $h-p$ Nitsche-type method

02/2013 Brugiapaglia, S.; Gemignani, L.
On the simultaneous refinement of the zeros of H-palindromic polynomials

01/2013 Arnold, D.N.; Boffi, D.; Bonizzoni,F.
Tensor product finite element differential forms and their approximation properties

56/2012 Ieva, F.; Paganoni, A.M.
Risk Prediction for Myocardial Infarction via Generalized Functional Regression Models

55/2012 Peng Chen, Alfio Quarteroni, Gianluigi Rozza
Uncertainty quantification of the human arterial network

54/2012 Ettinger, B., Perotto, S.; Sangalli, L.M.
Spatial regression models over two-dimensional manifolds

53/2012 Fumagalli, A.; Scotti, A.
An efficient XFEM approximation of Darcy flows in fractured porous media